Hysteresis in the Voltage Dependence of HCN Channels: Conversion between Two Modes Affects Pacemaker Properties

Roope Männikkö,[1] Shilpi Pandey,[2] H. Peter Larsson,[2] and Fredrik Elinder[1]

[1]Department of Neuroscience, The Nobel Institute for Neurophysiology, Karolinska Institutet, SE-171 77 Stockholm, Sweden
[2]Neurological Sciences Institute, Oregon Health and Science University, Beaverton, OR 97006

ABSTRACT Hyperpolarization-activated, cyclic nucleotide-gated (HCN) ion channels are important for rhythmic activity in the brain and in the heart. In this study, using ionic and gating current measurements, we show that cloned spHCN channels undergo a hysteresis in their voltage dependence during normal gating. For example, both the gating charge versus voltage curve, Q(V), and the conductance versus voltage curve, G(V), are shifted by about +60 mV when measured from a hyperpolarized holding potential compared with a depolarized holding potential. In addition, the kinetics of the tail current and the activation current change in parallel to the voltage shifts of the Q(V) and G(V) curves. Mammalian HCN1 channels display similar effects in their ionic currents, suggesting that the mammalian HCN channels also undergo voltage hysteresis. We propose a model in which HCN channels transit between two modes. The voltage dependence in the two modes is shifted relative to each other, and the occupancy of the two modes depends on the previous activation of the channel. The shifts in the voltage dependence are fast ($\tau \approx 100$ ms) and are not accompanied by any apparent inactivation. In HCN1 channels, the shift in voltage dependence is slower in a 100 mM K extracellular solution compared with a 1 mM K solution. Based on these findings, we suggest that molecular conformations similar to slow (C-type) inactivation of K channels underlie voltage hysteresis in HCN channels. The voltage hysteresis results in HCN channels displaying different voltage dependences during different phases in the pacemaker cycle. Computer simulations suggest that voltage hysteresis in HCN channels decreases the risk of arrhythmia in pacemaker cells.

KEY WORDS: HCN channel • voltage shift • voltage clamp • oocyte • arrhythmia

INTRODUCTION

Hyperpolarization-activated, cyclic nucleotide-gated (HCN) ion channels are important for rhythmic activity in the brain and in the heart, for resting membrane properties, for modulating synaptic transmission, and for limiting extreme hyperpolarizations (DiFrancesco, 1993; Pape, 1996; Santoro and Tibbs, 1999; Baruscotti and DiFrancesco, 2004). In thalamic-relay neurons in the brain and in the sino-atrial (SA) node of the heart, for example, the activation of HCN channels generates an inward cation current, I_h or I_f, that repetitively depolarizes the pacemaker cells from about −70 to −40 mV, which in turn triggers action potentials.

HCN channels belong to the super family of voltage-gated ion channels (Yu and Catterall, 2004), most members of which open in response to membrane depolarization. However, HCN channels open in response to membrane hyperpolarization. The voltage dependence of ion channels in this super family, including the HCN channels, is mainly due to the transmembrane movement of positive gating charges in the fourth transmembrane segment, S4, in response to changes in the transmembrane voltage (Aggarwal and MacKinnon, 1996; Larsson et al., 1996; Seoh et al., 1996; Yang et al., 1996; Keynes and Elinder, 1999; Männikkö et al., 2002). It is not known why the HCN channels open in response to membrane hyperpolarization rather than to depolarization (Larsson, 2002).

To elucidate how HCN channels function as pacemaker channels in driving the rhythmic firing of pacemaker cells, we studied the voltage dependence of two cloned HCN channels: the spHCN channel from sea urchin and the mammalian HCN1 channel. To study the voltage-sensing mechanism of spHCN channels, we measured gating currents that arise from the transmembrane movement of the gating charges (Armstrong and Bezanilla, 1973; Keynes and Rojas, 1974; Bezanilla et al., 1991). We found that the gating currents from spHCN channels undergo a hysteresis in their voltage dependence. We also found that the ionic currents from spHCN channels, as well as the ionic currents from HCN1 channels, display features indicating that the ionic currents also undergo a voltage hysteresis. For example, both the activation and tail kinetics change in response to negative prepulses. Therefore, we hypothesize that the mammalian HCN channels also undergo

Correspondence to Fredrik Elinder: fredrik.elinder@ibk.liu.se; or H. Peter Larsson: larssonp@ohsu.edu

Abbreviations used in this paper: HCN, hyperpolarization-activated, cyclic nucleotide-gated; SA, sino-atrial; wt, wild-type.

J. Gen. Physiol. © The Rockefeller University Press • 0022-1295/2005/03/305/22 $8.00
Volume 125 March 2005 305–326
http://www.jgp.org/cgi/doi/10.1085/jgp.200409130

hysteresis in their voltage dependence during physiological pacemaker activity. Based on the data obtained from our studies of mammalian HCN channels, we performed computer simulations of the pacemaker action potential in mammalian SA node cells. Our results suggest that the voltage hysteresis in mammalian HCN channels prevents arrhythmic behavior of pacemaker cells in the heart and the brain.

MATERIALS AND METHODS

Molecular Biology

The experiments were performed on hyperpolarization-activated spHCN channels (Gauss et al., 1998) from sea urchin (*Strongylocentrotus purpuratus*) expressed in *Xenopus laevis* oocytes. To study mammalian HCN channels, we used the mouse HCN1 channel with a stop codon introduced at position S391 to remove the cyclic nucleotide-binding site in the COOH terminus (Wainger et al., 2001). Site-directed mutagenesis, cRNA synthesis, and cRNA injection into *Xenopus laevis* oocytes were performed as described previously (Larsson and Elinder, 2000).

Electrophysiology and Solutions

To record the ionic currents, we used a two-electrode voltage-clamp technique, and to record the gating currents, we used either the two-electrode or the cut-open oocyte voltage-clamp technique, as described previously (Männikkö et al., 2002), with the CA-1B amplifier (Dagan Corp.). For the two-electrode recordings, we used a 100-K bath solution (in mM): 89 KCl, 15 HEPES, 0.4 $CaCl_2$, and 0.8 $MgCl_2$. In some experiments, we used a 1-K or 10-K bath solution, in which 88 or 79 mM KCl was changed to NaCl. To adjust the pH to 7.4, KOH (or NaOH for low K solutions) was added, yielding a final K concentration of ~100 mM. For the cut-open oocyte recordings, the solutions in the (extracellular) top pool and the guard pool were composed of (in mM) 107 KOH, 107 methanesulfonic acid, 10 HEPES, and 2 $CaCl_2$. The solution in the (intracellular) lower pool was (in mM) 110 KOH, 110 methanesulfonic acid, 10 HEPES, and 0.1 EGTA. The electronic cancellation of endogenous, linear capacitance transients was adjusted at +20 mV to avoid activating the gating currents of spHCN, which move at potentials more negative than 0 mV when measured from a positive holding potential. The recordings were made without any leak compensation, P/4 compensation, or averaging. For the quantitative analysis of the experiments, we used off-line digital leakage compensation. All experiments were performed at room temperature (20–23°C).

Voltage Protocols

To measure the size of the shift of the gating charge versus voltage curve, Q(V), due to the mode shift, we measured the Q(V) from a 0-mV and −80-mV holding potential. To study the time course for the voltage shift of the Q(V), we stepped to −80 mV for different durations, and then, to measure changes in the Qoff, we stepped back to a tail voltage between the $V_{1/2}$ for the Q(V)s of the two modes (−40 mV; Fig. 1 A). To study changes in the ionic tails due to the mode shift, we activated the channels at −80 mV for spHCN channels and −100 mV for HCN1 channels for different durations, and then we measured the tails at +50 mV (Fig. 1 B). To study the changes in the activation rate of the ionic current due to the mode shift, we activated the channels at −100 mV (V_{step} 1) for different durations, followed by a brief pulse to +80 mV to close the channels with as little recovery as possible from the mode shift. Then we reactivated the channel at −100 mV (Fig. 1 C). To measure the shift of the conductance versus voltage curve, G(V), due to the mode shift, we first activated the spHCN channels at −100 mV for different durations. This was then followed by voltage steps of 100-ms duration to different voltages to isolate the activation and the deactivation of the spHCN channels with as little change in mode as possible during the 100-ms voltage steps (Fig. 1 D). For the voltage ramps, we chose a speed for the fastest ramp that was so fast that most of the HCN channels would not undergo the mode shift (Fig. 1 E). Inter-episode time was 10 s for all protocols.

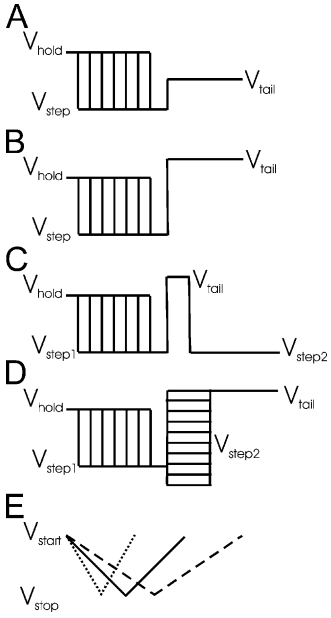

FIGURE 1. Voltage protocols to measure hysteresis. In the present investigation, different voltage protocols were used to measure the different effects of voltage hysteresis: (A) Q(V) shifts, (B) the development of tail current changes, (C) the development of activation current changes, (D) G(V) shifts, and (E) hysteresis during voltage-clamp ramps.

Computer Simulations

To explore spHCN channel kinetics, we used five models (shown in Fig. 5): (1) a simple, two-state model, (2) a linear five-state model developed by Hodgkin and Huxley (1952) for K-channel kinetics (the HH model), (3) a 10-state model developed by Altomare et al. (2001) for HCN channel kinetics (the Altomare model), (4) a linear four-state model, and (5) a circular, four-state model. Models 4 and 5 were developed in the present study. The rate constants in the models are described by the transition state theory:

$$\alpha = k_{1/2}\exp(-ze_0(V - V_{1/2})/kT) \quad (1)$$

$$\beta = k_{1/2}\exp(+ze_0(V - V_{1/2})/kT), \quad (2)$$

where $k_{1/2}$ is the rate constant at $V_{1/2}$ (i.e., when $\alpha = \beta$), z is the valence of the transition, e_0 is the elementary charge, V is the membrane voltage, k is Boltzmann's constant, and T is the absolute temperature. The values describing the rate constants are presented in Table I. For the Altomare model, we used the published values for z (1.02 and 0.94). For the other models, we set z to 1.0, which is close to the value for published HCN models (Zhang et al., 2000; Altomare et al., 2001). To compare the five models, we adjusted $V_{1/2}$ to yield a steady-state open probability of 50% at −45 mV when measured from a 0 mV holding potential (experimentally found in the present investigation for spHCN), and we adjusted $k_{1/2}$ values to generate a time course at −80 mV, which was compatible with the experimental data for spHCN channels (see Fig. 5 B). The Altomare model is a typical allosteric

TABLE I

Parameters for the Rate Constants Described by Eqs. 1 and 2 in Materials and Methods

	α/β			κ/λ					
	$V_{1/2}$	z	$k_{1/2}$	$V_{1/2}$	z	$k_{1/2}$	κ	λ	f
Four-state (circular)	−75	1	15	–	–	–	0.92	10	10.9
Four-state (linear)	−75	1	20	–	–	–	0.92	10	10.9
Two-state	−45	1	4.2	–	–	–	–	–	–
HH	−24	1	4.0	–	–	–	–	–	–
Altomare	−22	1.02	19.7	−125	0.94	4.8	–	–	2.24

α and κ are described by Eq. 1, and β and λ by Eq. 2.

model (see Hille, 2001) with two voltage-dependent processes (vertical and horizontal). For the calculations in this paper, the two voltage-dependent processes were equally adjusted with respect to $V_{1/2}$ and $k_{1/2}$ to best fit spHCN-channel currents.

For computer simulations of the pacemaker action potential, we used equations and parameters from the peripheral rabbit SA node (Zhang et al., 2000). Eq. 42 in Zhang et al. (2000) was corrected to

$$\tau_q = 10.1 \cdot 10^{-3} + 65.17 \cdot 10^{-3}/(0.57\exp(-0.08(V + 49)) + 0.24\exp(0.1(V + 50.93))) \quad (3)$$

to fit the experimental time constant shown in that paper. τ_q is a time constant for the kinetics of a 4-AP sensitive current. For the HCN channels in the SA node simulation, we used the HCN-channel model described in APPENDIX 1. The reversal potential was set to −10 mV, and the maximum HCN channel conductance was set to 6.9 nS (both values taken from Zhang et al., 2000).

RESULTS

In the present investigation, we studied gating properties of cloned HCN channels expressed in *Xenopus laevis* oocytes. The RESULTS section is divided in three main subsections: (I) gating- and ionic current measurements of spHCN channels, (II) ionic current measurements of mammalian HCN1 channels, and (III) computer simulations of an SA node cell to evaluate the effect of HCN-channel voltage hysteresis in pacemaker cells.

I. Studies of the Sea Urchin spHCN Channel

History-dependent Gating Currents. Previously, we showed that gating currents can be measured from wild-type (wt) spHCN channels when the ionic currents are blocked by the specific HCN-channel blocker ZD7288 (Männikkö et al., 2002; Fig. 2 A). Here, we report that the mutation P435Y in the pore region of spHCN channels (equivalent to position 449 in the Shaker K channel) eliminated the ionic currents while preserving the gating currents (Fig. 2 B). These gating currents were similar to those for ZD7288-blocked, wt spHCN channels (compare Fig. 2 A). Un-injected (control) oocytes that we studied with similar voltage protocols did not display any obvious capacitive gating currents. Fig. 2 C shows the (absence of) capacitive gating currents for a control oocyte in comparison to an oocyte expressing P435Y channels, thus demonstrating that the capacitive gating currents studied in the present investigation originated from the P435Y spHCN channel. In the following paragraphs, we will focus on the nonconducting P435Y mutation, but some data for ZD7288-blocked wt spHCN channels will also be presented to illustrate the similarities between P435Y channels and ZD7288-blocked wt spHCN channels.

To measure the gating charge transfer, we integrated the transient gating currents at different voltages. Fig. 2 D shows two examples of Q(V)s, measured from a holding potential of −10 mV: one for nonconducting P435Y channels and one for ZD7288-blocked, wt spHCN channels. The Q(V)s were fitted to Boltzmann curves. The average midpoints of the Q(V) were −58 ± 3 mV (n = 7) for P435Y channels and −58 ± 6 mV (n = 4) for ZD7288-blocked, wt spHCN channels. The midpoint for the G(V) in conducting wt spHCN channels was −42 ± 2 mV (n = 6). However, the voltage range over which the gating charge moves is strongly dependent on the holding potential. When measured from a holding potential of −80 mV (Fig. 2 E), the Q(V) for P435Y spHCN channels shifted +60 mV to +2 ± 3 mV (n = 4; Fig. 2 F). The maximum gating charge measured from the two holding potentials was similar (ΔQ_{max} = −16 ± 10%; n = 5). This small difference is most likely due to a small fraction of a slow gating charge transfer, which is hard to measure accurately. However, despite these small differences in maximum gating charge transfers, it is clear that the Q(V) drastically shifted along the voltage axis. Fig. 2 G shows normalized data from Fig. 2 F. A similar shift (+65 ± 10 mV; n = 3) was seen in the Q(V) for ZD7288-blocked, wt spHCN channels when held at −80 mV, compared with 0 mV. This Q(V) shift is most likely caused by slow gating transitions that, at intermediate voltages, are too slow to be measured. A true steady-state Q(V) measurement with infinite current resolution and very long voltage steps is expected to give the same Q(V) measured from the two holding potentials.

To estimate the time course of the Q(V) shifts, we used a double-pulse protocol (Fig. 1 A). We first stepped the membrane voltage for different durations

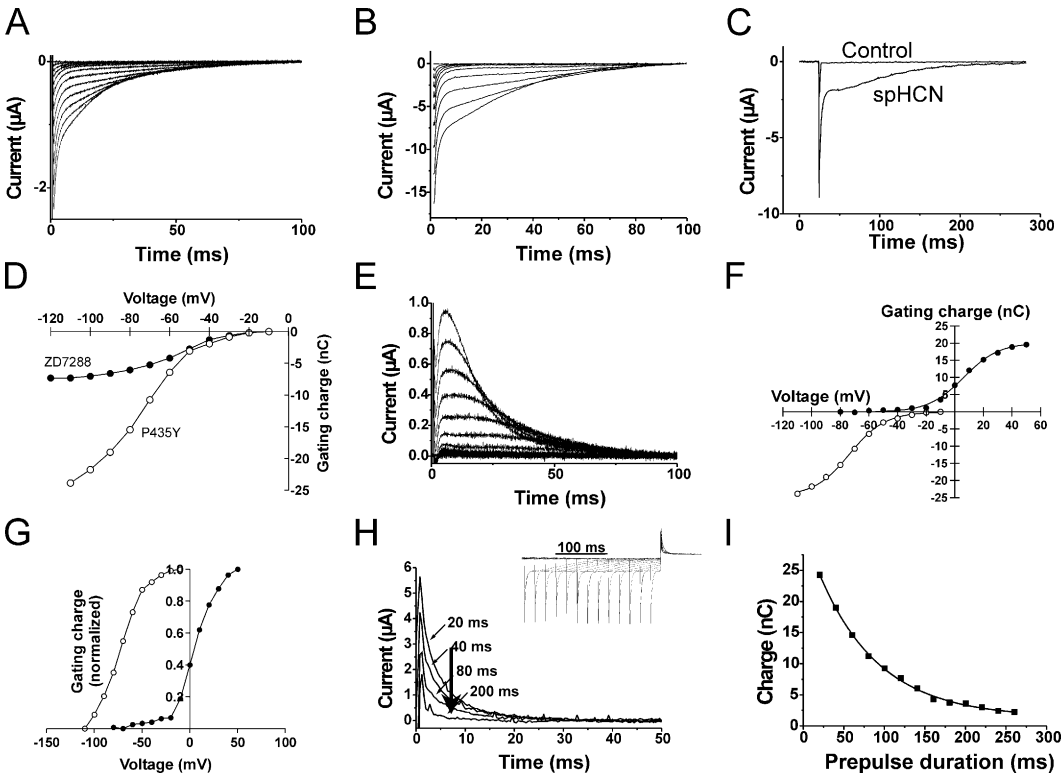

FIGURE 2. Q(V) shifts in spHCN channels. (A) Gating currents in response to voltage steps between −10 and −120 mV (ΔV = −10 mV) for ZD7288-blocked wt spHCN channels. Cut-open oocyte voltage-clamp technique; holding potential V_H = −10 mV. (B) Gating currents for a voltage protocol as in A for nonconducting P435Y spHCN channels. Two-electrode voltage clamp technique. (C) Currents in response to a voltage step to −80 mV from uninjected (control) oocytes and oocytes injected with nonconducting P435Y spHCN cRNA. Cut-open oocyte voltage-clamp technique. V_H = −10 mV. (D) Total gating charge (integral of gating currents) moved at the different voltage steps in (A) (●) and in (B) (○). (E) Gating currents in P435Y spHCN channels in response to voltage steps between −80 and +50 mV (ΔV = +10 mV), V_H = −80 mV. (F) Total gating charge (integral of gating currents) from P435Y spHCN channels, moved at different voltage steps from V_H = −10 mV (○) and from V_H = −80 mV (●), and fitted to $Q(V) = Q_{max}/(1 + \exp(-ze_0(V - V_{1/2})/kT)$. $V_{1/2}$ = −73 mV (○) and +6 mV (●). Q_{max} = −24.5 nC (○) and +20.1 nC (●), z = 2.1 for both curves. (G) The gating charge in F was normalized as $Q(V) = (Q(V) + Q_{min})/(Q_{max} - Q_{min})$. (H) Off (return) gating current of P435Y spHCN channels at −40 mV, after varying the lengths of activating pulses to −80 mV (raw data shown in inset). Note that the off (tail) gating charge paradoxically reduces (vertical arrow) while the on gating charge increases with increasing prepulse length (i.e., the shorter pulses curtail the on-gating currents). (I) The charge of the off-gating currents (from H) versus prepulse durations, fitted to an exponential decay with τ = 74 ms.

(20–250 ms) to a negative prepulse potential, −80 mV, to move most of the gating charge quickly. We then returned to an intermediate voltage, −40 mV, and measured the amount of gating charge that returned after each prepulse. If the gating charge returned according to the Q(V) measured from a holding potential of 0 mV, then we expected most of the gating charge to return at −40 mV. However, if, during the prepulse, a population of the channels shifted so that the gating charge returned according to the Q(V) measured from a holding potential of −80 mV, then we expected almost no gating charge to return from this population of channels. For short activation steps, most of the gating charge returned at −40 mV (Fig. 2 H, 20-ms trace). After longer and longer activation steps, the amount of gating charge that returned was successively smaller (Fig. 2 H, 40–260 ms). The Q(V) shift was unexpectedly fast. The time constant for the shift was 55 ± 9 ms (n = 3) at −80 mV (Fig. 2, H and I). A slow component with a similar time constant was found in the gating currents at −80 mV, suggesting that this gating charge component tracks the Q(V) shift. In similar experiments in which the Q(V) shift was measured in the opposite direction, the time constant was 94 ± 17 ms (n = 3) at positive voltages (+50 mV).

A similar Q(V) shift has been reported in depolarization-activated Na and K channels (Bezanilla et al., 1982; Olcese et al., 1997; Larsson and Elinder, 2000). However, in contrast to the spHCN channel, the Q(V) shift in Shaker K channels was found to be very slow (∼100 times slower; Olcese et al., 1997). In addition, the Q(V) shift in Shaker K channels was found to be coupled to slow inactivation (Olcese et al., 1997), while the Q(V) shift in spHCN channels was not accompanied by any apparent inactivation under these recording conditions (Männikkö et al., 2002).

History-dependent Tail Currents. The Q(V) shift in spHCN channels shows that the voltage dependence of the gating current (i.e., the movement of the voltage sensor S4) depends on the membrane holding potential. If the movement of the voltage sensor causes the ion pathway in these channels to open and to close, the ionic current should change its voltage dependence simultaneously, in parallel to the Q(V) shift. To test this hypothesis, we measured the ionic current after prepulsing HCN channels with negative voltage steps of varying durations (protocol in Fig. 1 B). After a brief negative pulse, the tail current was roughly a single exponential, while after a longer negative pulse, the tail current was slower and displayed a delay that was followed by an exponential decay (Fig. 3, A and B). The development of the delay in the tail currents for spHCN had a time constant of $\tau = 67 \pm 6$ ms ($n = 6$; Fig. 3 C). The time constant for the development of the tail delay was not voltage dependent at negative voltages from −100 to −140 mV (unpublished data). The time constant for the development of the tail delay was slower than the activation time constant at −80 mV (20 ms), but was similar to the time constant for the Q(V) shift. One explanation for the development of this delay is that spHCN channels have more than one open state, and they enter the additional open states only after the longer activating pulses and the Q(V) shift. The tail currents were fitted to the following equation:

$$(t) = I_o(1 - (1 - \exp(-t/\tau))^w) \qquad (4)$$

w varied from 0.95± 0.15 ($n = 4$), after the shorter activation pulses, to 3.6 ± 0.8 ($n = 4$), after the longest activation pulses (Fig. 3 D), indicating that spHCN channels have at least four open states. $\tau = 11.2 \pm 2.4$ ($n = 4$) for the first trace and $\tau = 10.2 \pm 3.2$ (n = 4) for the last trace (Fig. 3 B). A similar effect on the tail currents has been shown in native HCN channels (DiFrancesco, 1984).

For simple channel models, one would expect the Q(V) shift to result in a slowing of the time constant for the tail currents. However, the time constant for the tail currents did not drastically change at +50 mV. It was mainly the sigmoidicity of the tail currents that changed. However, for tail currents recorded closer to the $V_{1/2}$, the time constant for the tail currents changed drastically (Fig. 3, E and F). The time constant became slower after longer activation prepulses. For prepulses to −80 mV, the conversion of the tail currents at −15 mV from a quick to a slow decay had a time constant of $\tau = 104 \pm 24$ ms ($n = 3$). This time course is similar to the development of the delay in the tail currents at +50 mV. We show in APPENDIX 2 that the two effects, a slowing of the time constant and a change in the sigmoidicity of the tail currents, can both be a result of the Q(V) shift seen in the gating currents. The time-variant closing kinetics for the HCN channels is in sharp contrast to other noninactivating voltage-activated ion channels, which have closing kinetics that are independent of the length of the activating voltage pulse (Hahin, 1988; Zagotta et al., 1994).

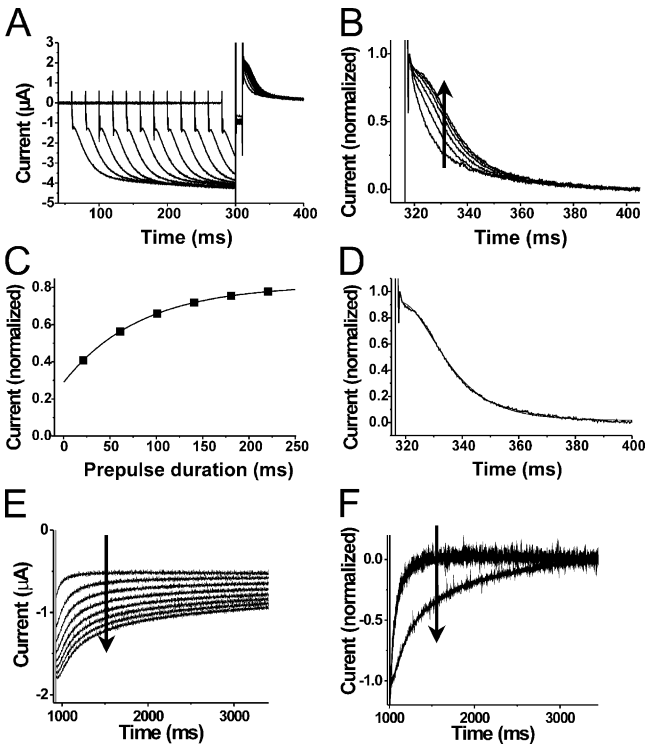

FIGURE 3. spHCN channels have multiple open states. (A) Development of a delay in the tail currents at +50 mV, in response to the increasing length of the −80 mV activation pulse. (B) Normalized tail current amplitudes from A. The prepulse length is increased with 40 ms for each trace. Arrow indicates increasing prepulse lengths. (C) Time course of development of the delay, measured as the tail current amplitude 10 ms after the onset of the tail potential (arrow in B), fitted with a single exponential with τ = 75 ms. (D) The tail currents were fitted to $I(t) = I_0(1 - (1 - \exp(-t/\tau))^w)$, where w = 3.2. (E) Tail currents at −15 mV for spHCN channels. The prepulse length is increased with 50 ms for each trace. Arrow indicates increasing prepulse lengths. (F) Normalized currents, first and last trace, from E. Arrow indicates increasing prepulse lengths. $\tau = 81.2 \pm 10.4$ ms ($n = 3$) for the first trace and $\tau = 639 \pm 32$ ms ($n = 3$) for the last trace.

History-dependent Activation Currents. If the Q(V) shift also alters the activation of the ionic current, then the kinetics of the ionic current should change after a voltage pulse that is long enough to shift the Q(V). To study the effects on the activation kinetics, we preactivated spHCN channels at −100 mV for different durations, then closed the channels quickly at +80 mV (without recovering the channels from the mode shift), and then reactivated the channels again at −100 mV (protocol in Fig. 1 C). We found that the activation kinetics of spHCN channels was prepulse dependent. After a brief negative prepulse to −100 mV (followed by a

brief pulse to +80 mV), the ionic current activated at −100 mV with a time constant of 13 ms, while, after longer negative prepulses, the ionic currents activated with a time constant of 8 ms (Fig. 4, A and B). The development of this speeding up of the activation time course had a time constant of $\tau = 91 \pm 31$ ms at −100 mV ($n = 4$; Fig. 4 C). This time constant is similar to the time constant for the development of the tail delay (compare Fig. 3 C) and the Q(V) shift (compare Fig. 2 I). In Fig. 4 D, the activation time constant is plotted for different activation voltages for spHCN channels after short (25 ms) and long (300 ms) prepulses to −100 mV. The voltage dependence of the activation time constant was almost identical for the two prepulses, but the effect of the longer prepulse could be described as a 30-mV shift in the voltage dependence of the activation time constant. The channels shifted back (recovered) to their original voltage dependence after longer voltage steps to depolarized potentials. We measured the time course of this recovery shift using a double-pulse protocol with a variable time at +80 mV between the two hyperpolarizing pulses (Fig. 4 E). The spHCN channels recovered to their original activation kinetics with a $\tau = 66 \pm 14$ ms at +80 mV ($n = 3$; Fig. 4 F).

The prepulse-dependent change in the activation kinetics for the spHCN channels is qualitatively different from most other voltage-activated ion channels. For example, Shaker K channels mainly display a change in the sigmoidicity of the activation time course, without a change in the activation time constant (Zagotta et al., 1994). Both native and cloned mammalian HCN channels have been shown to display this speeding up of activation kinetics, shown here in Fig. 4 for spHCN channels (DiFrancesco and Ferroni, 1983; DiFrancesco, 1984; Altomare et al., 2001). However, no explicit mechanism for the speeding up of the kinetics was suggested in these earlier studies. The changes in the kinetics of the ionic current, seen in both tail and activation currents in spHCN channels, are consistent with a Q(V) shift that alters the voltage dependence of the ionic current of spHCN channels.

A Four-state Model of the spHCN Channel. Our data show that, depending on the membrane holding potential, the voltage dependence of the gating charge movement in spHCN channels changes and that the kinetics and the voltage dependence of the ionic current change in parallel to the Q(V) shift. We propose a simple, four-state model that captures the essential features of the spHCN channel currents. This four-state model has two modes (I and II), each with a different voltage dependence (V_I and V_{II}) separated by 60 mV, and each with one open state (O) and one closed (C) state (see Fig. 5 A and APPENDIX 1). In mode I, the gating charge movement and the channel opening occur at very negative potentials, while in mode II, they are shifted to more depolarized potentials. The I→II transition is favored in the open states, while the II→I transition is favored in the closed states.

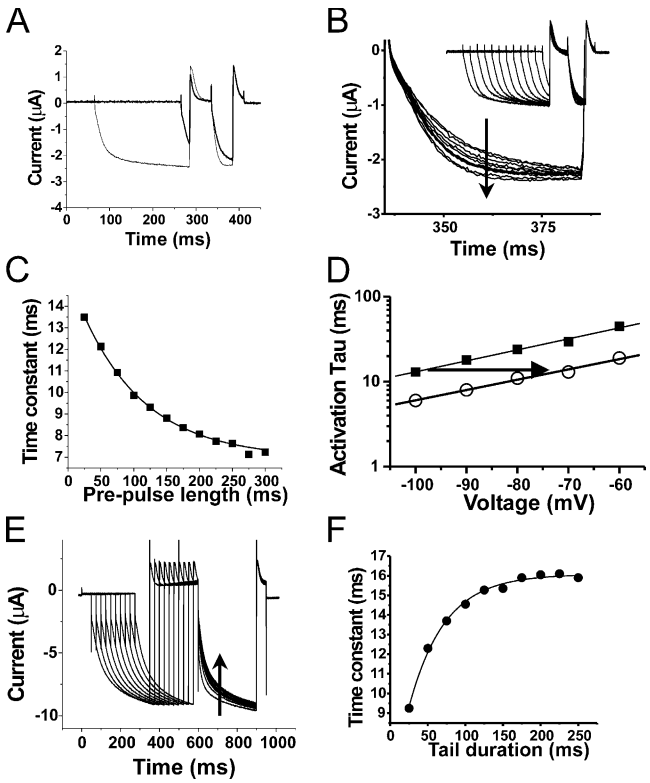

FIGURE 4. Activation kinetics is altered by negative prepulses. (A) A double-pulse protocol showing the change in both tail kinetics (at +80 mV) and activation kinetics (at −100 mV) induced by a 225-ms step to −100 mV versus a 25-ms step to −100 mV. Currents shown are the subtraction of the currents from the same cell in response to identical voltage protocols with and without 0.5 mM ZD7288. (B) Currents during the second −100-mV step in a double-pulse protocol (inset) used to measure the time course of the change in activation kinetics: −100 mV (step increase 25 ms), +80 mV for 50 ms, −100 mV for 50 ms, and +80 mV for 25 ms. Arrow indicates increasing prepulse lengths. (C) Time course of the change in activation time constant in B, fitted by a single exponential. $\tau = 73$ ms. (D) Activation time constant during the second step in B for different voltages during the second negative voltage step. The remainder of the double-pulse protocol was as in B. Activation time constant (■) after a 25-ms prepulse and (○) after a 300-ms prepulse. The data were fitted to $t = t_0 \exp(-zV/kT)$. (■) $z = 0.74 \pm 0.04$ and (○) $z = 0.70 \pm 0.04$. Arrow shows the voltage shift that superimposes the two lines (=28 mV in this cell). (E) Recovery of the activation time constant during the second negative voltage step in response to an increased duration of the step to +80 mV in the double-pulse protocol: −100 mV for 300 ms, +80 ms (25-ms step increase), −100 mV for 50 ms, and +80 ms for 25 ms. Arrow indicates increasing prepulse lengths. (F) Time constant during the second step to −100 mV in E after different durations at +80 mV. The data were fit to an exponential with $\tau = 58$ ms.

In Fig. 5 B, we compare our four-state model to three different models for HCN channel kinetics (described in Fig. 5 A): (1) a simple two-state model, (2) a linear

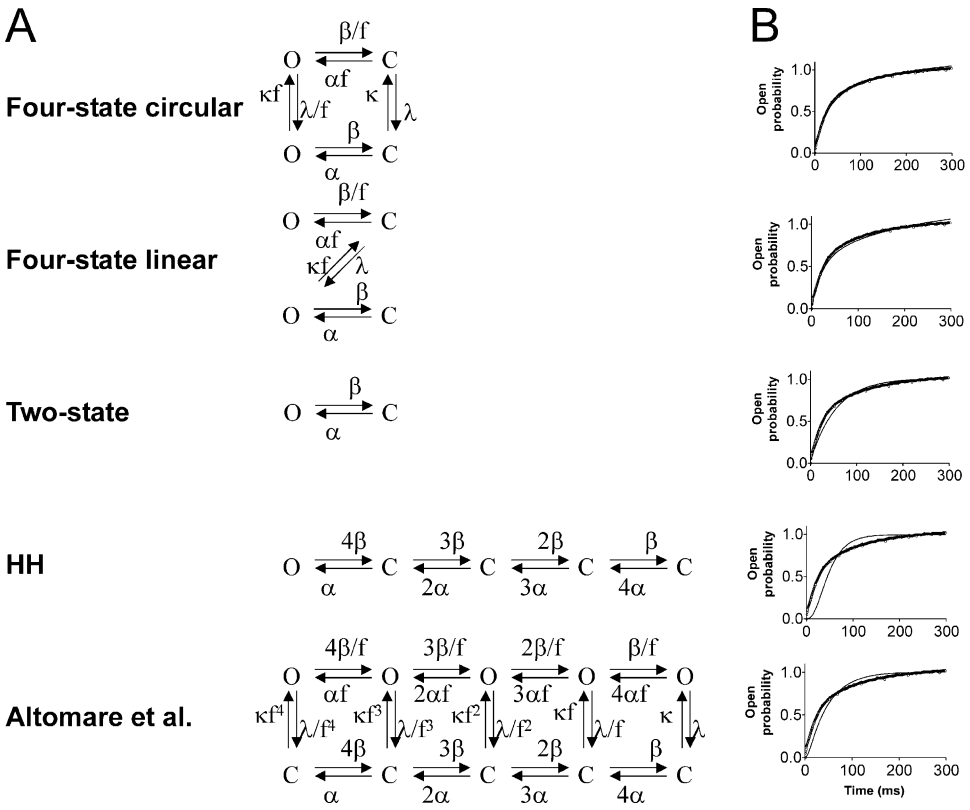

FIGURE 5. Kinetic models used in the present study. (A) O denotes open states, and C denotes closed states. The rate constants are described by Eqs. 1 and 2 in MATERIALS AND METHODS, with the values given in Table I. All models have a steady-state open probability of 50% at −45 mV. (B) To obtain similar activation rates, the models (continuous line) were adjusted to fit to experimental data (○) at −80 mV.

model similar to the HH model for K-channel kinetics (Hodgkin and Huxley, 1952), and (3) the Altomare model for HCN channel kinetics (Altomare et al., 2001). There are two variants of the four-state model: circular and linear. A description of the channel parameters for the models is found in MATERIALS AND METHODS and in Table I. Fig. 5 B shows conventional voltage-clamp currents for all five models at −80 mV. All models were constructed to give 50% steady-state open probability at −45 mV, and the time courses were tuned to give similar activation kinetics at −80 mV (thick line is experimental data). It should be noted that the two four-state models were superior to the other three models with respect to the activation kinetics. To test the models with respect to other spHCN channel data, we simulated gating currents, tail ionic currents, and activation ionic currents.

Fig. 6 (A–E) shows the Q(V) curves from $V_H = -80$ (right curve) and $V_H = 0$ (left curve) for all five models. Only the four-state models showed large Q(V) shifts that were comparable to the experimental data. The Q(V) shift for the circular four-state model was somewhat smaller than the experimental data. To increase the Q(V) shift for the circular four-state model, the difference between $V_{1/2}$ for the two modes is simply increased. However, incorporating more open and closed states in the circular four-state model, as suggested by the tail currents (see DISCUSSION), could also increase the Q(V) shifts. In this early, simplified four-state model, we have, therefore, not suggested a larger difference than 60 mV in the $V_{1/2}$. Furthermore, the time course of the Q(V) shift for the circular four-state model, as determined by mimicking the protocol in Fig. 2 H, was similar to the experimentally obtained time course (see Fig. 6 F and Fig. 2 I). The time constant (96 ms) almost directly reflects the inverse of the rate constant for the mode shift ($(100\ \text{ms})^{-1}$). Most importantly, the two-state model (and the HH model) predicts a qualitatively different (opposite) gating charge development at −45 mV. The two-state model predicts an increase in Off gating charge with increased prepulse length, while the four-state model predicts a decrease in Off gating charge with increased prepulse length, as was found experimentally.

Fig. 7 (A–E) shows the tail currents for the models as measured in Fig. 3. Only the four-state models displayed a change in tail kinetics, in which the tails became slower after longer activation steps. Fig. 7 F shows the time course of the tail development. Although the simple four-state models were able to replicate a change in tail current kinetics, they could not replicate the sigmoidicity of the ionic currents since there are not enough open and closed states in these simplified models. However, future models that extend the four-state models will most likely be able to fit the details of the ionic current kinetics (see DISCUSSION and APPEN-

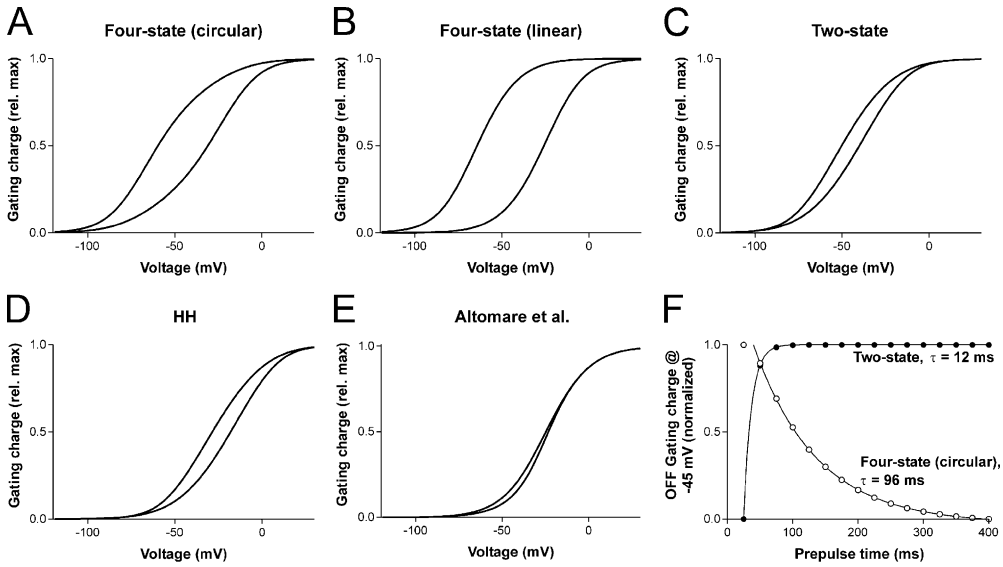

FIGURE 6. Q(V) curves simulated for the models in Fig. 5. The gating charge, Q, was measured as the amount of charge that moved during a 200-ms pulse. (A–E) Simulations of the models in Fig. 5. Holding voltage V_H = 0 mV for the left curve in each panel, V_H = −80 mV for the right curve. (F) Time courses of the OFF gating charge at −45 mV after different prepulses to −100 mV (protocol similar to that shown in Fig. 2 H).

DIX 2). The other models did not display any change in tail current kinetics after the longer activation steps, in contrast to the four-state models.

Fig. 8 (A–E) shows the activation currents of the models simulated with the same voltage protocols as in Fig. 4. Only the four-state models showed a speeding up of the activation kinetics, similar to the experimental data. Fig. 8 F shows the time development of the change in activation kinetics, similar to the experimental data (Fig. 4 C). Fig. 8 (G and H) shows that the voltage dependence of the activation kinetics has the same slope after a short or a long prepulse but that the activation kinetics shifted ~20 mV along the voltage axes (see arrow). This shift is similar to the shift in the experimental data (Fig. 4 D). It is interesting to note that the voltage shifts in the activation kinetics (20–30 mV) were much smaller than the Q(V) shifts (60 mV), both for the four-state models and the experimental data. One possible explanation for this discrepancy is that the rates of opening and closing were not much faster

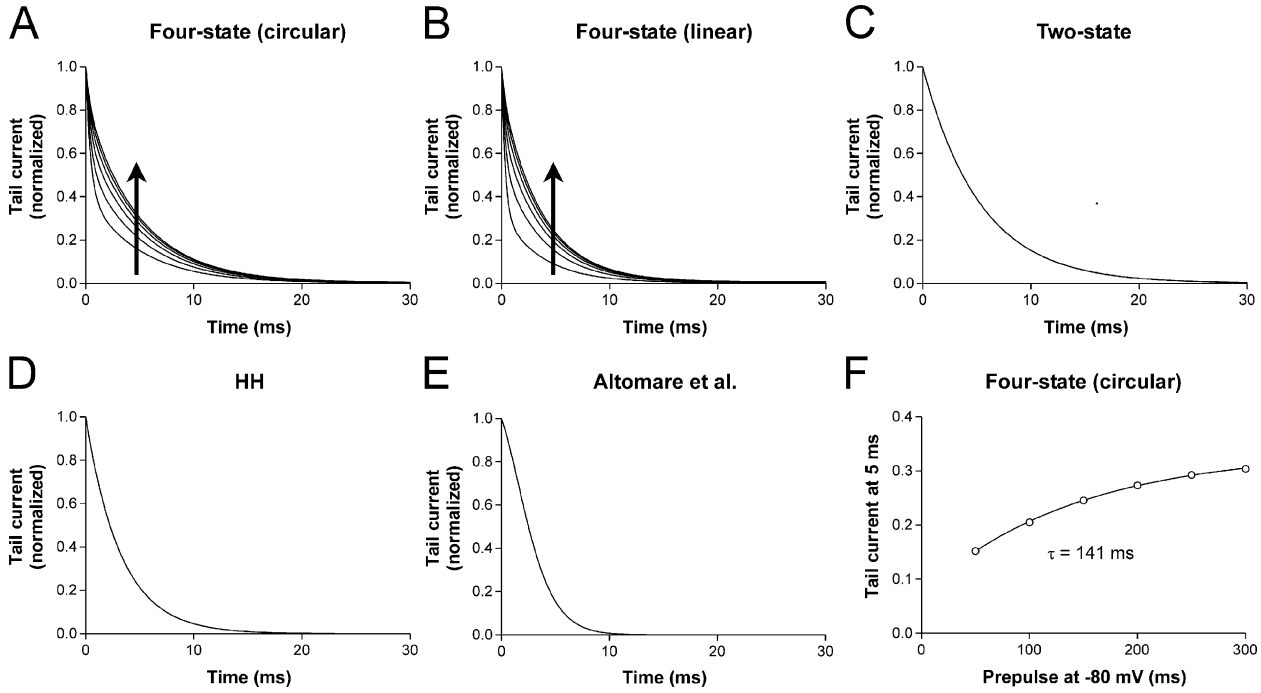

FIGURE 7. Simulated tail currents. (A–E) Simulations of the models in Fig. 5. Holding voltage is 0 mV. The channel-opening prepulse is −120 mV for 50, 100, 150, 200, 250, or 300 ms, and the following tail current is simulated at +50 mV. The tail currents that are shown are normalized to 1 for the first data point. Arrows indicate increasing prepulse lengths. (F) Development of the tail current for the model in A.

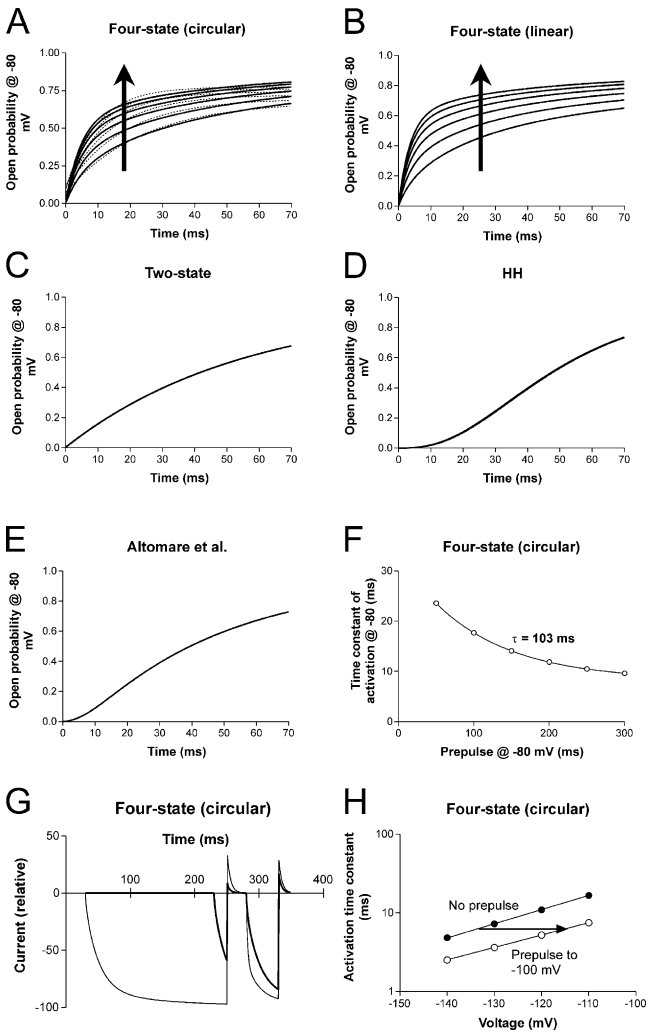

FIGURE 8. Simulated prepulse-dependent activation kinetics. (A–E) Double-pulse protocol simulations of the models in Fig. 5. Holding voltage is 0 mV. Prepulse to −100 mV for 50, 100, 150, 200, 250, or 300 ms, followed by a closing step at +80 mV for 30 ms, and then followed by a second step to −100 mV. The activation kinetics shown were measured during the second pulse to −100 mV. Arrows indicate increasing prepulse lengths. See G for an example of a simulation. (F) Development of the activation kinetics for the simulations in A measured as single exponentials (see dotted lines in A). (G) Simulations shown for prepulse lengths of 25 and 225 ms. (H) Voltage dependence of activation time constants following no prepulse or a 225-ms long prepulse to −100 mV. The slopes correspond to z = 0.91 (with prepulse) and z = 1.04 (no prepulse). See legend to Fig. 4 for an explanation of voltage protocol.

than the rates for the voltage shifts, making it impossible to measure the activation kinetics without some channels also undergoing the voltage shifts. Taken together, our linear and circular four-state models are significantly better than the other models at simulating the effects of holding potentials and prepulses of different durations that were found in the experimental data.

History-dependent G(V) Curves. It has earlier been reported that extremely long hyperpolarizing pulses have to be applied to measure true steady-state G(V) curves for HCN channels (Santoro et al., 2000). Shorter hyperpolarizing voltage steps result in more hyperpolarized G(V)s, while longer hyperpolarizing voltage steps result in more depolarized G(V)s. This is due to an unusually slow activation component in HCN channels at intermediate voltages. For example, the currents in response to a voltage step to −40 mV equilibrate very slowly in spHCN channels (Fig. 9 A). This slow equilibration made the current markedly different in amplitude when the spHCN channels were briefly prepulsed to −100 mV versus just stepped to −40 mV (Fig. 9 A). Our modeling suggests that the slowly activating component is due to the Q(V) shift in spHCN channels (Fig. 9, B–F).

In our four-state model, for shorter voltage pulses, spHCN channels mainly equilibrate between the open and closed states in mode I, giving a G(V) with a $V_{1/2}$ = −75 mV. For longer pulses, spHCN channels reach a true equilibrium, and the G(V) is halfway between the $V_{1/2}$ of mode I and mode II. In contrast, G(V)s measured with shorter voltage steps from a negative holding potential (or after a negative prepulse) have a $V_{1/2}$ = −15 mV, because in this case, the spHCN channels mainly equilibrate between the open and closed states in mode II.

To visualize the possible different behaviors of spHCN channels, we measured the voltage dependence of the ionic current after prepulsing HCN channels with negative voltage steps of varying duration (protocol in Fig. 1 D). These prepulses were followed by a standard voltage protocol (see MATERIALS AND METHODS) to determine the voltage dependence of the conductance, G(V) (Fig. 10, A and B). Fig. 10 C shows G(V) curves for spHCN channels after prepulses of different durations to −80 mV. The G(V) shifted to more positive voltages after the negative prepulses (Fig. 10 D, τ = 39 ± 6 ms, ΔV = 53 ± 4 mV; n = 4). For less negative prepulses that did not open the channels maximally, the G(V) shift was much slower. However, the rate of the G(V) shift saturated at more negative voltages (unpublished data), suggesting that the G(V) shift is intrinsically voltage independent but is coupled to the voltage-dependent opening of the channel. The Na/K selectivity ratio, measured as the reversal potential, was not altered by the G(V) shift (unpublished data). The voltage shift of the G(V) in spHCN channels was similar both in magnitude and in time course to the voltage shift of the Q(V), suggesting that the G(V) shifts are due to the Q(V) shifts.

Fig. 10 (E–H) shows the results from simulations using voltage protocols similar to those in the experiments. Any type of voltage-gated channel model gives

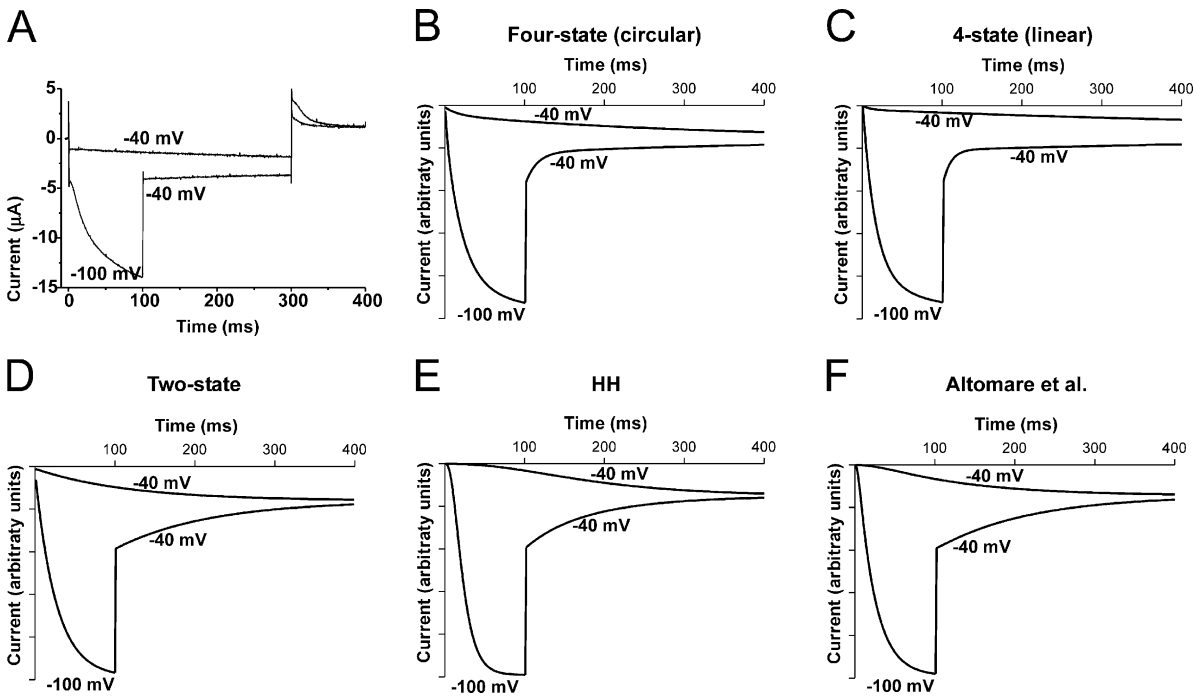

FIGURE 9. Slow equilibration at −40 mV in spHCN channels. (A) Currents in response to voltage steps to −40 mV, with or without a 100-ms prepulse to −100 mV. V_H = −10 mV. 100-K bath solution. (B–F) Computer simulations of the different models shown in Fig. 5, in response to the protocol used in A.

G(V) shifts that are dependent on the prepulse length. However, neither the experimentally obtained magnitude nor the time course of the G(V) shift was displayed by the HH model or the Altomare model. Both of these models predicted shifts of 10–12 mV, and both predicted that >95% of the shift would occur within 75 ms. In contrast, both variants of the four-state model showed larger and relatively slower shifts. In addition, only the four-state model showed a voltage-independent G(V) shift at more negative voltages. Fig. 10 I shows simulated G(V) shifts for the four-state model and the two-state model for four different prepulse potentials (−60, −100, −140, and −180 mV). The time constants for the G(V) shifts are plotted in Fig. 10 J. While the four-state model saturates at negative voltages, the two-state model does not. Thus, the experimental data strongly support the four-state model.

Hysteresis in Voltage Dependence. HCN channels are best known for their contribution as pacemaker channels in rhythmically firing cells. For a rhythmically firing cell like an SA node cell, the membrane potential alternates between hyperpolarized (−70 mV) and depolarized potentials (+40 mV). An SA node cell spends hundreds of milliseconds at each of these potentials during each pacemaker cycle. Using our four-state model with two modes for HCN channels, we predicted HCN channels to exhibit a voltage dependence during the depolarizing phase of the pacemaker cycle that is different from the voltage dependence during the hyperpolarizing phase. We tested this prediction by measuring the conductance of spHCN channels during voltage ramps.

The conductance of spHCN channels displayed voltage hysteresis in response to slow voltage ramps (shown in Fig. 11 A). It is important to note that any voltage-dependent channel displays hysteresis when the voltage is ramped faster than the opening kinetics of the channel and that the hysteresis decreases for very slow ramps. However, the hysteresis in spHCN channels is qualitatively different from the hysteresis in other voltage-gated ion channels. In the Shaker Kv channel, we found that the hysteresis monotonically decreased with a decreasing ramp speed for all ramp rates tested (Fig. 11 B). In contrast, in spHCN channels, the hysteresis did not decrease and, for some ramp speeds, even appeared to increase with decreasing ramp speed (Fig. 11 A). For even slower ramp speeds, the hysteresis did decrease for spHCN, but even for a ramp speed as slow as 10 mV/s, there was a clear hysteresis. However, in response to very slow voltage ramps, we expect HCN channels not to display any voltage hysteresis because they have time to reach equilibrium at all voltages.

That the channels did not reach complete equilibrium even for these slow ramps does not contradict our finding of a voltage-independent Q(V) shift with a time constant of τ = 75 ms in spHCN channels. In our four-state model, the Q(V) shift is preceded by a voltage-dependent step, and therefore, the occupancy of the

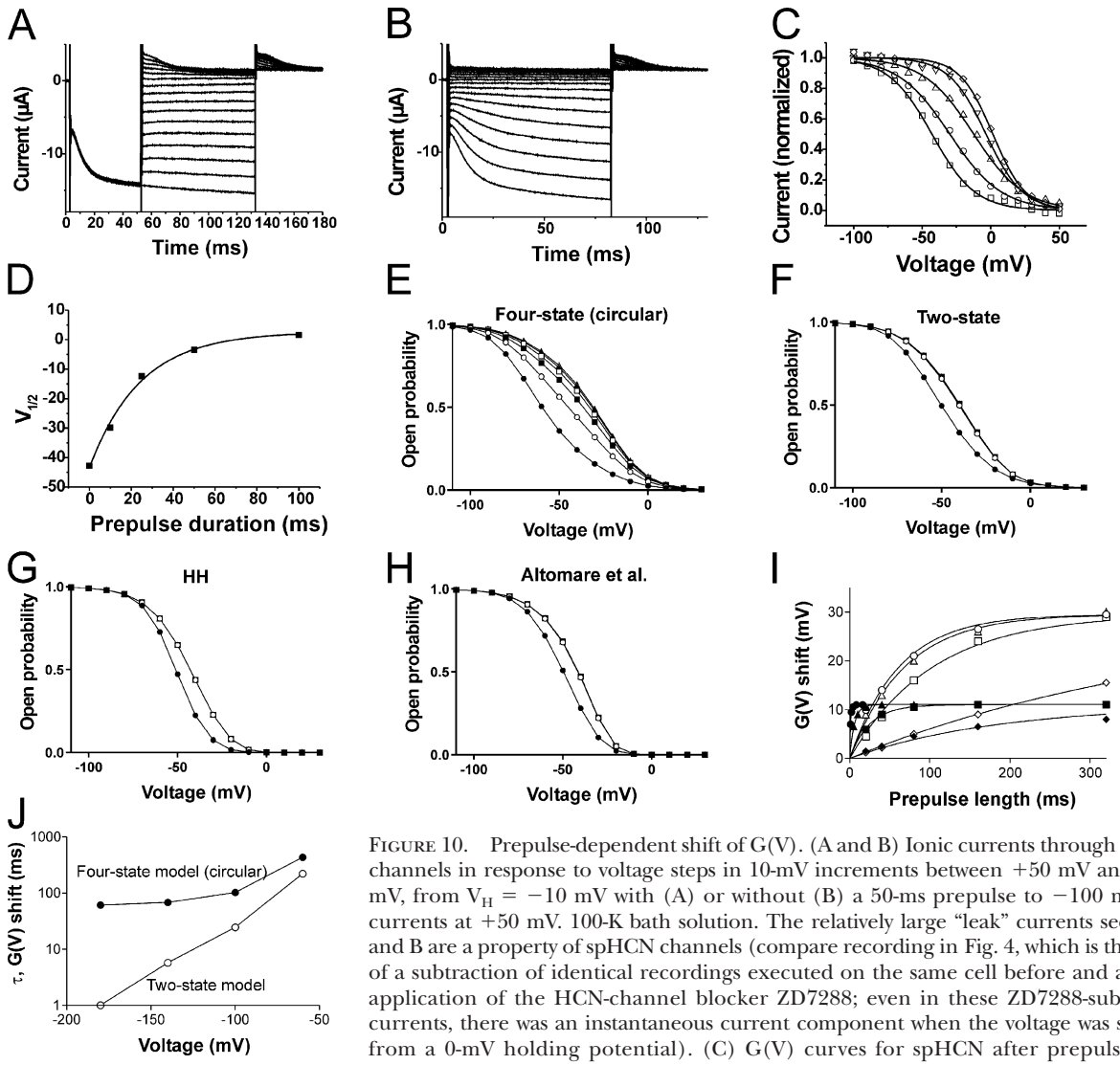

FIGURE 10. Prepulse-dependent shift of G(V). (A and B) Ionic currents through spHCN channels in response to voltage steps in 10-mV increments between +50 mV and −100 mV, from V_H = −10 mV with (A) or without (B) a 50-ms prepulse to −100 mV. Tail currents at +50 mV. 100-K bath solution. The relatively large "leak" currents seen in A and B are a property of spHCN channels (compare recording in Fig. 4, which is the result of a subtraction of identical recordings executed on the same cell before and after an application of the HCN-channel blocker ZD7288; even in these ZD7288-subtracted currents, there was an instantaneous current component when the voltage was stepped from a 0-mV holding potential). (C) G(V) curves for spHCN after prepulses with durations of 0 (□), 10 (○), 25 (△), 50 (▽), and 100 (◇) ms, measured from an instantaneous tail current at +50 mV. Fitted to $G(V) = A + B/(1 + \exp(-ze_0(V - V_{1/2})/kT)$. $V_{1/2}$ = −43, −30, −12, −3, +2. z = 1.59, 1.33, 1.37, 1.87, and 2.10. 100-K bath solution. (D) $V_{1/2}$ versus prepulse duration from C, fitted with a single exponential with τ = 24 ms. (E–H) Computer simulations of G(V) shifts for the models in Fig. 5. Holding potential is 0 mV followed by prepulses to −100 mV for 0, 75, 150, 225, 300, and 375 ms (from left to right), followed by equilibrium steps of 200 ms to the voltages indicated on the x axis. Compared with the other models, the four-state model exhibits the largest and the slowest shifts. (I) G(V) shifts for the four-state (open symbols) and the two-state (closed symbols) models for different prepulse potentials (circle, −180 mV; triangle, −140 mV; square, −100 mV; diamond, −60 mV). The continuous curves are best fits of single exponentials through origin. (J) Time constants from I. Note that the time constants from the four-state model, in contrast to the two-state model, levels out as was found in the experiments.

state from which spHCN channels undergo the Q(V) shift is voltage dependent. This voltage dependence slows down the apparent time constant of the Q(V) shifts at voltages at which a majority of the channels have not undergone the voltage-dependent transitions. However, in response to very slow voltage ramps, we expect HCN channels not to display any voltage hysteresis because they have time to reach equilibrium at all voltages.

Neither the HH model nor the Altomare model predicted currents compatible with the experimental results. Both models showed decreased hysteresis with reduced ramp speed (Fig. 11, C–F). To quantify the hysteresis, we measured the voltage separation between the upward and downward limbs at 50% relative conductance (relative to the conductance at −100 mV). Fig. 11 G shows experimental data for spHCN and simulated data for the four models, and Fig. 11 H shows experimental data for Shaker channels. The four-state model best describes the spHCN data, while the other models best describe the Shaker data. It should be noted that the four-state model also started to show reduced hysteresis for the slowest ramp simulations, in contrast to the experimental data. This discrepancy be-

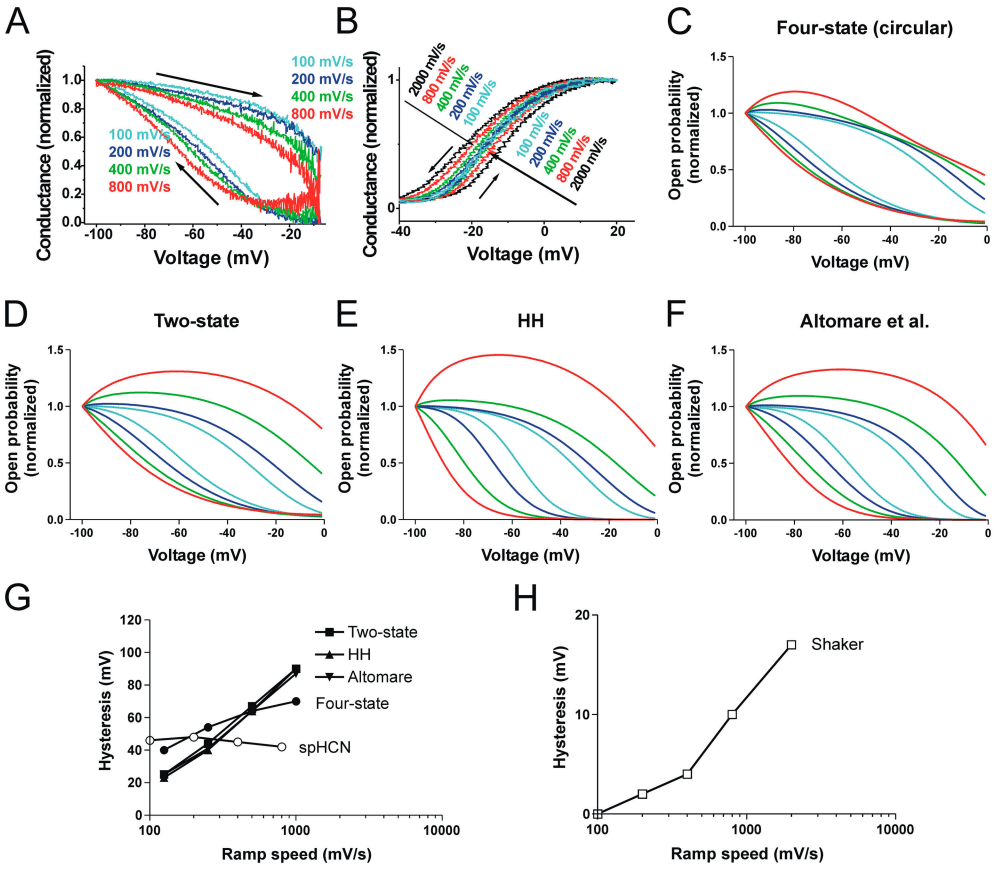

FIGURE 11. Voltage ramps. (A) Conductance of spHCN channels during voltage ramps from −10 mV to −100 mV, and back to −10 mV, using different ramp speeds. 100-K bath solution. The conductance was normalized to 1 at −100 mV. (B) Conductance of Shaker channels during voltage ramps from −80 mV to +20 mV, and back to −80 mV, using different ramp speeds. The conductance was normalized to 1 at +20 mV. 1-K bath solution. Note that with a slower ramp speed, voltage hysteresis decreases in Shaker channels, whereas it increases in spHCN channels. With slower voltage ramps, the two limbs in the G(V) curve approach each other in Kv channels, but in HCN channels, the two limbs are well separated even for slow ramps. (C–F) Computer simulations of voltage-ramp currents for the models in Fig. 5. The ramp speed is 125, 250, 500, 1,000, and 2,000 mV/s (from periphery to center). (G and H) Hysteresis measured as the voltage separation between the upward and downward limbs at 50% relative conductance (relative to the conductance at −100 mV).

tween our model and the data most likely is due to the limited number of states (only four) in the models. If more states are introduced (see DISCUSSION and APPENDIX 2), as we suggest based on data from the tail experiments, we expect the model to more closely match the experimental hysteresis data at slow ramp speeds.

cAMP Does Not Play a Major Role in Generating the Voltage Shifts. Wang et al. (2002) showed that HCN2 channels undergo small voltage shifts of the G(V), caused by the higher affinity of HCN2 channels for cAMP in the open state than in the closed state. However, several experimental findings do not support cAMP binding as the major cause of the G(V) shift reported in the present study. (a) cAMP does not shift the G(V) along the voltage axis in spHCN channels but increases the maximum conductance of spHCN channels (Gauss et al., 1998). (b) Our recordings in *Xenopus laevis* oocytes were made in saturating concentrations of cAMP, as judged by the absence of inactivation in our spHCN recordings. (c) The slowing of tails and the development of a delay in tail currents were also seen in spHCN channels in excised patches perfused with saturating cAMP concentrations (unpublished data) and in spHCN channels that had their COOH terminus deleted, including the cAMP-binding site (Fig. 12). These COOH terminus–truncated channels had a stop codon introduced at residue 472 (Vemana et al., 2004), located at the COOH-terminal end of S6. These truncated channels did not express at high enough levels for reliable recording of gating currents.

II. Studies on the Mammalian HCN1 Channel

We concluded above that the spHCN channel displays a hysteresis in voltage gating. We based our conclusion mainly on gating current measurements, supplemented by several types of ionic current measurements from spHCN channels. However, we have not been able to measure gating currents from the mammalian HCN channels, most likely because of the lower expression and slower channel kinetics of the mammalian HCN channels compared with the spHCN channels. Therefore, to test whether mammalian HCN channels also

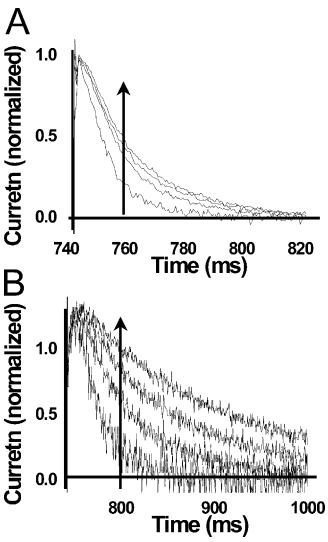

FIGURE 12. The change in tail kinetics is present in a COOH terminal–deleted spHCN channel. (A) Tail currents in Δ472 spHCN channels at +50 mV after increasingly longer (62.5–625 ms) activation prepulses to −150 mV in 1-K solution. Arrow indicates increasing prepulse lengths. (B) Tail currents at 0 mV after increasingly longer activation prepulses to −150 mV in 100-K solution. Arrow indicates increasing prepulse lengths. Note that the tails mainly develop a sigmoidal delay in A but mainly become slower in B after longer-activating prepulses.

display voltage hysteresis, we investigated a number of ionic current parameters of HCN1 channels to determine whether the Q(V) shift is reflected in the ionic currents from mammalian HCN1 channels.

History-dependent Tail Currents. We have shown that voltage hysteresis in spHCN channels and in computer-simulated HCN channels gives rise to prepulse-dependent tail kinetics, in sharp contrast to other noninactivating, voltage-activated ion channels that have closing kinetics that is independent of the length of the activating voltage pulse. If mammalian HCN1 channels display voltage hysteresis similar to those of spHCN channels, then the tail kinetics of mammalian HCN channels should be prepulse dependent, similar to the tail kinetics of spHCN channels.

In Fig. 13 A, we show that the mammalian HCN1 channels have prepulse-dependent tail currents, similar to the spHCN channels (Fig. 13 B). After a brief negative pulse, the tail currents from HCN1 channels were roughly single exponential, while after longer negative pulses, the tail currents displayed a delay followed by an exponential decay (Fig. 13, A and C). The development of the delay in the tail currents had a time constant of $\tau = 250 \pm 76$ ms ($n = 3$; Fig. 13 D). Similar to spHCN channels, the development of a sigmoidicity in the tail kinetics of HCN1 channels was not accompanied by a slowing of the time constant of the tail decay at depolarized potentials. $n = 1.2 \pm 0.4$ ($n = 3$) after the shorter activation pulses and $n = 2.6 \pm 0.8$ ($n = 3$) after the longest activation pulses, while $\tau = 49.0 \pm 8.2$ ms ($n = 3$) for the first trace and $\tau = 51.3 \pm 3.2$ ms ($n = 3$) for the last trace (Fig. 13 C). However, for tail currents recorded closer to the $V_{1/2}$, the time constant for the decay of the tail currents changed drastically in HCN1, similar to the tail currents in spHCN channels (Fig. 13, E and F). Both of these behaviors, an increase

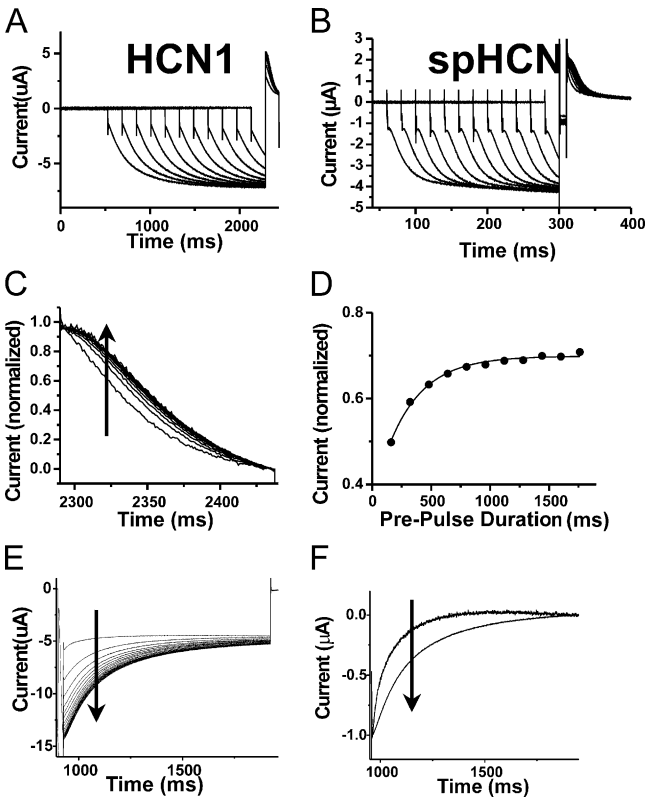

FIGURE 13. History-dependent, tail current kinetics. A similar development in (A) HCN1 channels and (B) spHCN channels, of a delay in the tail currents at +50 mV in response to the increasing length of the activation pulse. Pulse potential: −100 mV (A) and −80 mV (B). Extracellular K concentration: 10 mM (A) and 100 mM (B). (C) Normalized tail current amplitudes from A, showing the slowing of the tail kinetics. Arrow indicates increasing prepulse lengths. (D) Time course of the development of the delay, measured as the tail current amplitude, 10 ms after the onset of the tail potential (arrow in C), fitted with a single exponential with $\tau = 250$ ms. (E) Tail currents at −80 mV for HCN1 after increasing prepulses to −160 mV. The prepulse length is increased with 50 ms between each trace. Arrow indicates increasing prepulse lengths. (F) Normalized currents, first and last trace, from E. Arrow indicates increasing prepulse lengths. $\tau = 98.3 \pm 5.2$ ms ($n = 3$) for the first trace and $\tau = 211 \pm 16$ ms ($n = 3$) for the last trace.

in the sigmoidicity and a slowing of the time constant for the tail currents, can be explained by a voltage shift of the Q(V) (see APPENDIX 2).

Wang et al. (2002) have shown that cAMP binding to HCN2 channels can alter the voltage dependence of HCN2 channels and can slow channel closing. However, the HCN1 channels used in our studies had their COOH terminus deleted, including the cAMP-binding site. Therefore, the changes in the tail currents of mammalian HCN1 channels reported here occurred in the absence of cAMP binding. These changes are very similar to the changes in the tail currents from spHCN channels, suggesting that HCN1 and spHCN channels are gated similarly.

History-dependent Activation Time Course of Ionic Currents. For the spHCN channel, we showed that voltage hysteresis gives rise to prepulse-dependent activation kinetics. If mammalian HCN1 channels display a voltage hysteresis that is similar to that in spHCN channels, then the activation time course of mammalian HCN channels should be prepulse dependent, similar to the activation time course in spHCN channels.

To study the hysteresis effects on the activation kinetics, we preactivated HCN1 channels for different durations at −100 mV, then closed the channels quickly at +80 mV (without recovering the channels from the mode shift), and then reactivated the channels. Fig. 14 A shows that after a brief negative pulse, the ionic current for HCN1 channels activated at −100 mV with a bi-exponential time course. The smaller time constant was 197 ms, and the larger time constant was 717 ms. The amplitude of the faster component was 65 ± 8% of the total amplitude. After longer negative pulses, the ionic currents activated with a bi-exponential time course. The smaller time constant was 91 ms, and the larger time constant was 349 ms. (Fig. 14 A). The change in the activation time course in HCN1 channels was very similar to the changes in the activation time course of spHCN channels (Fig. 14, A and B). In HCN channels, the development of the speeding up of the activation time course had a time constant of τ = 257 ± 30 ms at −100 mV, in 10 mM K (n = 3; Fig. 14, C and D). This time constant (Fig. 14 D) was similar to the time constant for the development of the tail delay (compare Fig. 13 D). In Fig. 14 E, the fast-activation time constant is plotted for different activation voltages after a 160-ms prepulse and after a 1600-ms prepulse to −100 mV. The voltage dependence of the activation time constant was not significantly different after short versus long prepulses (note parallel lines in Fig. 14 E), but the effect of the longer prepulse can be described as a voltage shift of ∼12 mV (Fig. 14 E). It should be noted that even though the apparent shift in voltage dependence of activation kinetics is small, the mode shift underlying this apparent shift is most likely much larger. For example, in computer simulations of the four-state model, for a mode shift of 60 mV, the shift in activation kinetics was only 20 mV. The HCN1 channels shifted back (recovered) to their original voltage dependence after longer voltage steps to depolarized potentials. We measured the time course of this recovery using a double-pulse protocol with a variable time at +80 mV between the two hyperpolarizing pulses (Fig. 14, F and G). The HCN1 channels recovered to their original activation kinetics with a τ = 381 ± 86 ms at +80 mV (n = 5; Fig. 14 H).

The mammalian HCN1 channels displayed changes in ionic current behavior similar to those of the spHCN channel, both in tail and in activation current kinetics,

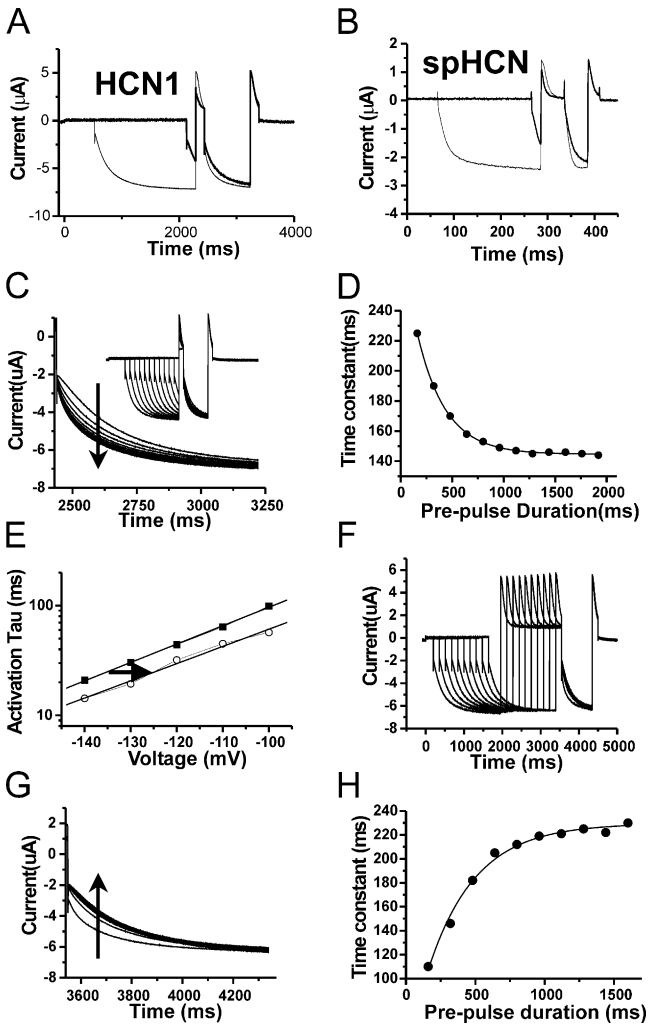

FIGURE 14. History-dependent activation kinetics. A similar change in both (A) HCN1 channels and (B) spHCN channels in tail kinetics and activation kinetics induced by a long-versus-short activation step in a double-pulse protocol. Activation potential: −100 mV (A) and −80 mV (B). Tail potential: +80 mV. (C) Currents from HCN1 channels during the second −100-mV step in a double-pulse protocol (inset), used to measure the time course of the change in activation kinetics: −100 mV (step increase 160 ms), +80 mV for 150 ms, −100 mV for 750 ms, and +80 mV for 150 ms. Arrow indicates increasing prepulse lengths. (D) Time course of the change of activation constant in C fitted by a single exponential. τ = 352 ms. (E) Activation time constant during the second step in C for different voltages during the second negative voltage step. The remainder of the double-pulse protocol was as in C. Activation time constant (■) after a 160-ms prepulse and (○) after a 1,600-ms prepulse. The data were fitted to $t = t_0\exp(-zV/kT)$. (■) z = 0.96 ± 0.02 and (○) z = 0.90 ± 0.06. Arrow shows the voltage shift that superimposes the two lines (=12 mV in this cell). (F) Recovery of the activation time constant during the second negative voltage step in response to an increased duration of the step to +80 mV in the double-pulse protocol: −100 mV for 1,600 ms, +80 mV (durations of 160–1,600 ms, in 160-ms step increase), −100 mV for 750 ms, and +80 ms for 160 ms. (G) Enlargement of the currents during the second step to −100 mV in F. Arrow indicates increasing prepulse lengths. (H) Time constant during the second step to −100 mV in E after different durations at +80 mV. The data were fit to an exponential with τ = 380 ms.

in response to prepulses of different duration, suggesting that mammalian HCN1 channels undergo a voltage hysteresis similar to the voltage hysteresis in spHCN channels.

Hysteresis in Voltage Dependence. Voltage hysteresis made HCN1 channels behave very differently after a depolarizing prepulse compared with after a hyperpolarizing prepulse. For example, the currents in response to a voltage step to −70 mV were markedly different in amplitude when the HCN channels were prepulsed to −120 mV versus just stepped to −70 mV, due to very slow current kinetics at −70 mV (Fig. 15 A). spHCN channels displayed a similar slow equilibration at intermediate voltages (Fig. 15 B). The very slow opening and closing at voltages close to $V_{1/2}$ or more positive than $V_{1/2}$ were well simulated by the four-state model with voltage hysteresis, but not by the other HCN channel models. We hypothesize that this slow equilibration is due to a voltage shift of the Q(V) (i.e., voltage hysteresis) in the channels that have opened, which in turn causes more channels to open by mass action. The voltage hysteresis caused the conductance of HCN1 channels to display an unusual hysteresis in response to slow voltage ramps (Fig. 15 C), similar to the hysteresis in spHCN channels (Fig. 15 D). Any voltage-dependent channel displays hysteresis when the voltage is ramped faster than the opening kinetics of the channel. However, the hysteresis in HCN channels is qualitatively different from that in other voltage-gated ion channels. Both the HCN channels and the four-state model showed a window of ramp speeds in which the hysteresis was relatively constant, while Kv channels and the other models showed monotonically decreasing hysteresis, with decreasing ramp speeds.

Mode Shift in HCN-channel Gating: A Possible Molecular Mechanism. In HCN1 channels, the time course for the development of the delay in the tail currents was dependent on the external K concentration, with high concentrations of external K slowing the development of the delay (Fig. 16, A and B). These results suggest that the permeant ions may affect the rate of voltage hysteresis. In support of this hypothesis, an addition of 1 mM Cs^+ to the 100 mM KCl external solution blocked the majority of the inward ionic currents and sped up the development of the delay in the tail currents (Fig. 16 C). The development of the tail currents had a time constant of $\tau = 67 \pm 6$ ms, in 1 mM K^+ ($n = 6$; Fig. 16 D). These findings suggest that the delay of the tail currents is governed by the occupancy of K^+ in a binding site in the pore and that external Cs^+ prevents external K^+ from accessing the pore. The K^+ dependence of the hysteresis in the HCN1 channels is reminiscent of the K^+ dependence for slow inactivation in Kv channels (López-Barneo et al., 1993), and the Q(V) shift seen in the HCN channels is similar to the Q(V) shift associated with slow inactivation in Shaker K channels (Olcese et al., 1997). Thus, despite the lack of visible inactivation in the HCN channels that we investigated, a molecular rearrangement similar to that of Kv channels during slow inactivation may underlie the Q(V) and G(V) shifts in HCN channels.

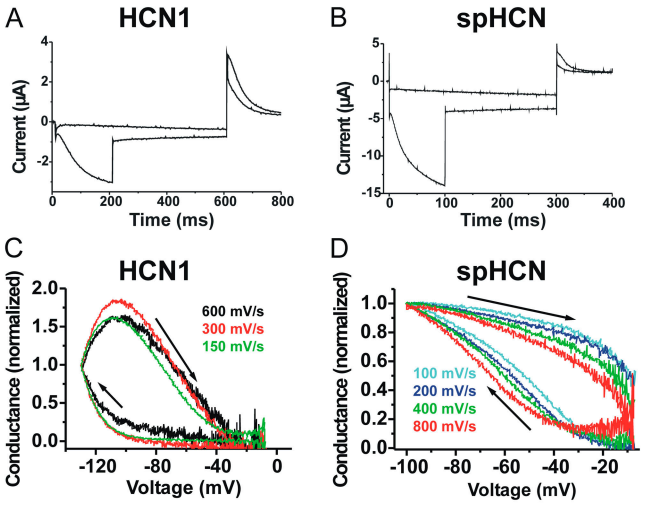

FIGURE 15. Prepulse-dependent activation and voltage-ramp currents. Slow equilibration at voltages close to $V_{1/2}$ in both (A) HCN1 channels and (B) spHCN channels. Currents in response to voltage steps (−70 mV [A] and −45 mV [B]), with or without prepulses to −120 mV (200 ms) for HCN (A) and −100 mV (100 ms) for spHCN channels. (B). $V_H = -10$ mV. 1-K bath solution (A) and 100-K bath solution (B). (C) Conductance (G = I/V) of HCN1 channels during voltage ramps from −10 to −130 mV, and back to −10 mV, using different ramp speeds. (D) Conductance (G = I/V) of spHCN channels during voltage ramps from −10 to −100 mV, and back to −10 mV, using different ramp speeds. 100-K bath solution.

III. Computer Simulations: A Physiological Role of Hysteresis in Pacemaker Activity

The four-state model proposed for the spHCN channel also describes most of the experimental findings for the HCN1 channel. Our model is composed of two modes (I and II), with two states (open and closed) in each mode (shown in APPENDIX 1). Upon hyperpolarization, the channel activates from the closed state to the open state in mode I. After ∼100 ms in the open state, the channel switches from mode I to mode II. When the channel is later deactivated at depolarized potentials, it closes via the closed state in mode II, to the closed state in mode I.

At physiological K concentrations, the mode shift in HCN1 channels is faster ($\tau \approx 100$ ms; Fig. 16) than the duration of a thalamic relay neuron oscillation or a cardiac action potential, suggesting that HCN1 channels undergo a mode shift during these types of rhythmic firing. This mode shift, or hysteresis, in the voltage dependence of a pacemaker channel is a feature that is

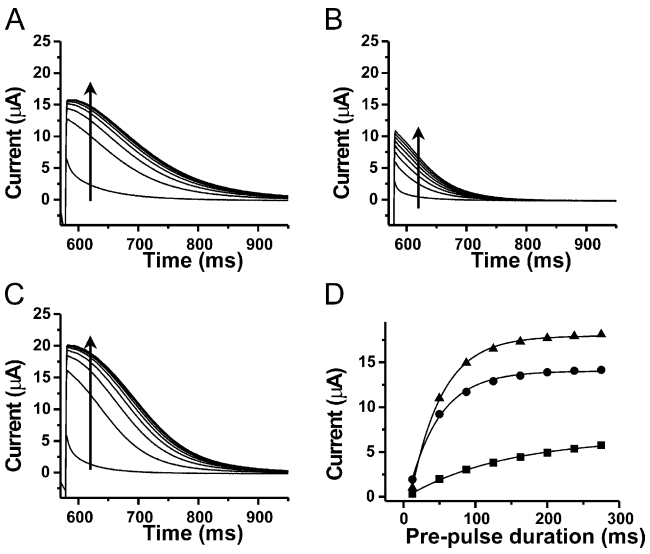

FIGURE 16. External K affects voltage hysteresis. Tail currents at +50 mV after different durations (12.5–275 ms, Δt = 37.5 ms) of a −160 mV activation pulse in 1-K (A), 100-K (B), and 100-K + 1 mM CsCl (C) bath solutions. Arrows indicate increasing prepulse lengths. (D) Time course of the development of the current delay in HCN1 channels. 1-K (●), 100-K (■), and 100-K + 1 mM CsCl (▲) bath solutions. Time constants are 43, 145, and 44 ms, respectively.

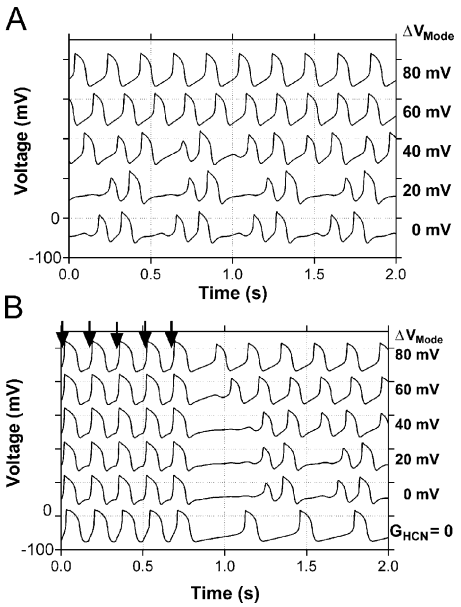

FIGURE 17. Hysteresis in HCN channels prevents arrhythmia. (A) Computer simulation of a model of an SA node cell (Zhang et al., 2000), incorporating the HCN channel model described in MATERIALS AND METHODS. Simulations were made with different values of the ΔV_{mode} (0, 20, 40, 60, and 80 mV). $V_{1/2}(I) = -75 - \Delta V_{mode}/2$, $V_{1/2}(II) = -75 + \Delta V_{mode}/2$. (B) Computer simulations with an external pacemaker stimulating at 6 Hz (arrows). Stimulating current was −100 pA for 30 ms.

beneficial during rhythmic firing. During the hyperpolarizing phase of the action potential, HCN channels do not open until the cell reaches very negative voltages, thus preventing HCN channels from interfering with the recovery from inactivation of Na and Ca channels. In the interval between action potentials, HCN channels remain open, pushing the cell above the threshold to fire the next action potential.

To test the effect of hysteresis in pacemaking quantitatively, we performed computer simulations of the cardiac action potential in the peripheral SA node (Zhang et al., 2000), incorporating our model HCN channels (see MATERIALS AND METHODS and APPENDIX 1) with different amounts of hysteresis (voltage shifts of 0, 20, 40, 60, and 80 mV between modes I and II; Fig. 17 A). The simulations with HCN channels without any voltage hysteresis (the nonmode shift model) displayed an irregular spacing of the action potential, i.e., cardiac arrhythmia. The addition of a minor voltage hysteresis (a 20-mV voltage shift) in the HCN channels had no effect on the arrhythmia. However, for voltage shifts of 40 mV, the arrhythmia became less frequent, and for even larger voltage shifts, the arrhythmia disappeared completely, suggesting that voltage hysteresis in HCN channels stabilizes the rhythmic firing of the SA node and prevents cardiac arrhythmia from occurring. Sympathetic stimulation (more positive V_I and V_{II}, which leads to an increase in the firing frequency) or stimulation by an external pacemaker (Fig. 17 B) removed the arrhythmia in the nonmode shift model. In addition, directly after the cessation of the pacemaker stimulation, there was a long gap before the next action potential for the nonmode shift model or for a model without any HCN channels, a gap that was much longer than for the model containing HCN channels with a large voltage hysteresis (Fig. 17 B). These behaviors of the nonmode shift model are reminiscent of those seen in sick sinus syndrome (Tchou and Chung, 2000). Our results suggest that this syndrome, in some cases, may be caused by defects in HCN channels that alter the voltage hysteresis in HCN channels.

The arrhythmic behavior found for the nonmode shift model is in contrast to what has been reported in other computer simulation studies (e.g., Zhang et al., 2000). A reason for this discrepancy may be the slightly different ground rates $k_{1/2}$ (the rates for a specific transition at the voltage for which the forward and backward rates are equal) for the channel kinetics. The effect of different ground rates $k_{1/2}$ on the rhythmic behavior is illustrated in Fig. 18 A, where $k_{1/2}$ is changed (logarithmically) from 5 to 500 s^{-1} during a 5-s simulation. The parameters used in the model by Zhang et al. (2000) are the same as in the left part of Fig. 18 A, which represents the nonarrhythmic region of the simulation. A broad, clearly arrhythmic window is seen in the simulation. However, when the simulation was re-

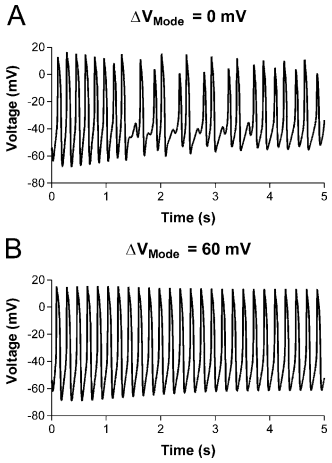

FIGURE 18. Voltage hysteresis prevents arrhythmia. Computer simulations of the SA-node model developed by Zhang et al. (2000). The HCN channels were replaced by our HCN-channel model (MATERIALS AND METHODS). During the 5-s simulation, $k_{1/2}$ changed from 5 to 500 s^{-1}. The change was logarithmic, which means that $k_{1/2} = 50$ in the middle of the trace. (A) No mode shift. (B) Mode shift = 60 mV. Note the clearly arrhythmic firing for the nonmode shift model at intermediate rate constants.

peated with a mode shift of 60 mV, the arrhythmic behavior was abolished (Fig. 18 B), demonstrating the stabilizing effect of the HCN mode shift on the rhythmic firing of the pacemaker cell.

DISCUSSION

We have shown that HCN channels display behaviors that are qualitatively different from those in a traditional Hodgkin-Huxley type channel. In spHCN channels, negative prepulses (a) shift the Q(V) curve, (b) alter the tail currents, and (c) speed up the activation kinetics. We were unable to record gating currents from HCN1 channels, but the ionic currents from HCN1 channels were similar to the ionic currents from spHCN channels. Some of these ionic current behaviors have previously been noted in cloned (Santoro et al., 2000; Altomare et al., 2001) and native (DiFrancesco and Ferroni, 1983; DiFrancesco, 1984) HCN channels, but no explicit mechanism had been proposed to explain these behaviors.

We propose a model for HCN channels in which HCN channels exist in two modes with different voltage dependences. In the proposed model, the voltage dependence of the HCN channels depends on their prior activity. If the HCN channels are kept open for >100 ms, the voltage dependence of activation shifts to more depolarized potentials, which tends to keep the channels open. If they are kept closed for >100 ms, the voltage dependence of activation shifts to more hyperpolarized potentials, which tends to keep them closed. This shift in the voltage dependence creates a hysteresis in the voltage dependence of HCN channel activity. We suggest that this hysteresis is important for the physiological functioning of HCN channels in rhythmic firing cells.

The binding of cAMP to the COOH terminus of HCN channels has been shown to induce small voltage shifts (Wang et al., 2002). However, in the present study, the voltage shifts due to the mode shifts were much larger than the cAMP-induced voltage shifts. We propose that the mode shifts are distinct from the cAMP-induced voltage shifts, since the mode shifts were measured either in an spHCN channel (where cAMP is not shifting the G(V) along the voltage axis) or in a cAMP-independent HCN1 channel (see MATERIALS AND METHODS).

The Four-state Model

The basic features of HCN channels described in the present investigation (except the sigmoidal tail, which requires at least four open states) can be described by a simple four-state model with two different modes (I and II), each with a different voltage dependence (V_I and V_{II}) and each with one open state (O) and one closed state (C) (see Fig. 19 A and APPENDIX 1). The gating charge movement and the channel opening occur at very negative potentials in mode I, but they are shifted to more depolarized potentials in mode II. The I→II transition is favored in the open states, while the II→I transition is favored in the closed states. The proposed model better explains the experimental findings than does a simple two-state model, the Hodgkin-Huxley type model, or the Altomare model (Altomare et al., 2001).

In our initial modeling, we used two variants of the four-state model: one circular and one linear (Fig. 5). In the circular variant, there are two pathways between the two modes, while in the linear variant, there is only one pathway (between O_I and C_{II}) where the backward and forward rates are equal (10 s^{-1}). The kinetic properties of the two variants are very similar (however, not identical), but their molecular interpretations are different. In the circular variant, the voltage-dependent transition in mode I moves the same gating charge as that in the voltage-dependent transition in mode II. In the linear variant, the two transitions move different gating charges, as if S4 moves first one step, and then S4 moves a second step after the voltage-independent step. Experimentally, we have found that the two gating charge transitions carry a similar amount of charge (Fig. 2 F). The circular variant predicts that one of the transitions moves all the gating charges, while the linear variant predicts that the first transition carries only half of the gating charge. The linear variant predicts, therefore, two components of gating current, where the slow component cannot be faster than ~100 ms (=the mode shift time constant). However, we have not found any evidence for such a large, slow component in the gating currents at very negative potentials (Fig. 2). Thus, we conclude that the circular variant of our model best describes the experimental data.

A more complete model of HCN channels that takes into account all of the kinetic details of the HCN cur-

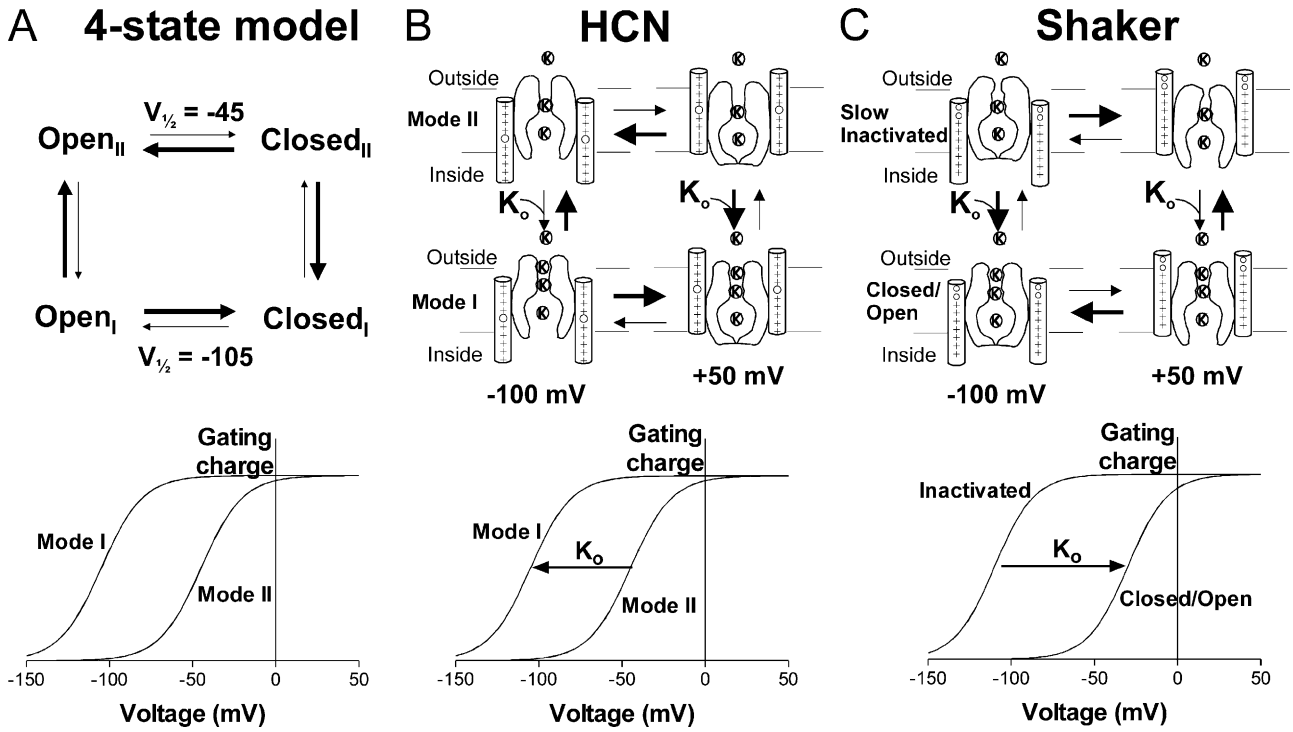

FIGURE 19. A four-state model for HCN channel gating. (A) Scheme for HCN kinetics. $V_{1/2}$ is the voltage at which open-to-closed and closed to-open transitions are equal. Molecular models for voltage hysteresis in (B) HCN channels and (C) Shaker K channels. See DISCUSSION "Molecular Mechanism for Mode Shift" for description.

rent, for example, the shape of sigmoidal delay of the activation and tail currents, calls for much more kinetic data and more detailed data analyses. We envision that a future model of spHCN channels that takes into account all of the kinetic features of the spHCN current and the Q(V) shift will be a 20-state model, with each of the two modes being an "Altomare-type" 10-state model (see APPENDIX 2).

Slowing Versus Sigmoidicity during Activation

The prepulse-dependent change in the activation kinetics for the HCN channels is qualitatively different from other voltage-activated ion channels. Cole and Moore (1960) showed that the activation kinetics of depolarization-activated ion channels changes with the holding potential. This "Cole-Moore" effect is mainly displayed as a change in the sigmoidicity of the activation time course, without a change in the activation time constant (Zagotta et al., 1994).

The Cole-Moore effect has been interpreted as follows: the holding potential causes a redistribution of the channels among the many different closed states, so that from more hyperpolarized holding potentials, the channels must go through more closed states before opening. These transitions through closed states lead to more sigmoidal activation kinetics from the more hyperpolarized holding potentials, without a change in the time constant of activation (this is only true for a channel with identical independent subunits). However, in our study, the changes in HCN channel kinetics were qualitatively different. The main effect of the negative prepulses in HCN channels was a clear speeding up of the activation kinetics. Both native and cloned mammalian HCN channels have been shown to display both a speeding up of activation kinetics, shown here in Fig. 4 for spHCN channels, and the classical Cole-Moore shifts (DiFrancesco and Ferroni, 1983; DiFrancesco, 1984; Altomare et al., 2001). This speeding up of the activation kinetics has been interpreted in terms of HCN channel kinetics that "require multi-reactions with nonidentical and/or nonindependent gating subunits" (DiFrancesco and Ferroni, 1983). However, no explicit mechanism for the speeding up of the kinetics was suggested in these earlier studies. The HCN channels used in our study are composed of identical subunits, which suggests that the prepulse effects seen here are not due to nonidentical gating subunits. Although we cannot rule out cooperative effects (i.e., nonindependent gating subunits) on the kinetics of HCN channels, the changes in the kinetics of the ionic current, seen in both tail and activation currents in HCN channels, are consistent with a Q(V) shift that alters the voltage dependence of the opening and closing of HCN channels.

Molecular Mechanism for the Mode Shift

What is the molecular mechanism for the voltage hysteresis? We suggest that the Q(V) shift and hysteresis in HCN channels are mediated by a concerted conformational change in all subunits. As noted in RESULTS, a similar voltage shift in the Q(V), as we reported for HCN channels, has been linked to slow inactivation in Shaker K channels (Olcese et al., 1997). Therefore, we hypothesize that the conformational changes leading to voltage hysteresis in HCN channels are similar to the concerted conformational changes in the extracellular part of voltage-gated K channels that lead to slow (C-type) inactivation (Ogielska et al., 1995; Panyi et al., 1995; Liu et al., 1996; Loots and Isacoff, 1998; Larsson and Elinder, 2000). However, in HCN channels, the voltage shift does not lead to any apparent inactivation. Channel inactivation, as such, is not an absolute requirement for the Q(V) shift, even in Shaker channels (the Shaker mutant T449V/I470C undergoes the voltage shift without inactivating; Olcese et al., 2001). Furthermore, we found that the voltage shift in HCN1 channels is modulated by extracellular K ions, in a manner similar to the slow inactivation in Shaker K channels (López-Barneo et al., 1993). This finding suggests that the voltage shifts in HCN and Shaker K channels are caused by a similar mechanism. Therefore, we hypothesize that in both HCN and Shaker K channels, the opening of the activation gate leads to additional conformational changes in the pore, which are modulated by extracellular K, and that these conformational changes stabilize S4 in its current position (Fig. 19, B and C). This stabilization may be due to a reorientation of S4 relative to the pore or a change in the interface surface between S4 and the pore. These conformational changes stabilize S4 in the outward position in mode I and the inward position in mode II. In this model, external K stabilizes the open state of Shaker K channels, thereby favoring the depolarized shifted Q(V) in Shaker K channels, while external K stabilizes the open state in mode I in HCN channels, thereby favoring the hyperpolarized shifted Q(V) in HCN channels. The reason for not observing voltage hysteresis in Shaker K channels is that the channels simultaneously undergo slow inactivation (unless the T449V/I470C mutations are present, thus preventing closure of the inactivation gate). However, in HCN channels, the Q(V) shift (i.e., the mode shift) is not accompanied by any apparent inactivation, which results in voltage hysteresis in the ionic currents of HCN channels.

In contrast to HCN1 channels, the hysteresis in spHCN channels did not display any K dependence (unpublished data). The reason for the difference in K dependence between spHCN and mammalian HCN1 channels is not clear. The P loops of the two channels are different at a number of positions, suggesting that there are different K binding sites in the pore/vestibule or that the K binding sites in HCN1 and spHCN channels have different affinities. It has earlier been shown that the ion selectivity of spHCN channels has a different K dependence than the ion selectivity of mammalian HCN channels (Gauss et al., 1998; Ludwig et al., 1998).

Both spHCN channels and HCN2 channels have been shown to display some kind of inactivation. Shin et al. (2004) have suggested that HCN2 channels display a prepulse-dependent inactivation that is cAMP dependent. This type of inactivation has not been demonstrated for HCN1 channels. All of the HCN1 recordings in this study were done on HCN1 channels with their cAMP-binding domains deleted. In spHCN channels, the ionic current displays a time-dependent decrease in the current that can be abolished by a high concentration of cAMP (Gauss et al., 1998). This type of inactivation is not apparent in recordings from spHCN channels in intact *Xenopus laevis* oocytes, which have relatively high intracellular levels of cAMP (Männikkö et al., 2002). Therefore, we suggest that the voltage hysteresis is not linked to the inactivation seen at low cAMP in spHCN channels. In support of this hypothesis, we have shown that noninactivating spHCN channels without a cAMP-binding domain still display voltage hysteresis (Fig. 12).

The Role of Hysteresis for Pacemaker Activity

The mode shift in HCN channels is faster (≈100 ms) than the duration of a thalamic relay neuron oscillation or a cardiac action potential, suggesting that HCN channels undergo a mode shift during these types of rhythmic firing. This mode shift, or hysteresis, in the voltage dependence of a pacemaker channel is a feature that is beneficial during rhythmic firing. During the hyperpolarizing phase of the action potential, HCN channels do not open until the cell reaches very negative voltages, thus preventing HCN channels from interfering with the recovery of Na and Ca channels from inactivation. In the interval between action potentials, HCN channels remain open, pushing the cell above the threshold to fire the next action potential. Based on the equivalent role of HCN channels as pacemaker channels in cardiac and thalamic pacemaker cells (Clapham, 1998; Luthi and McCormick, 1998), hysteresis in HCN channels may play a similar role in thalamic neurons during, for example, delta wave oscillations. During delta wave oscillations (1–4 Hz oscillations with plateau potentials lasting >100 ms), thalamic neurons experience slowly alternating hyperpolarized and depolarized membrane potentials. We expect that HCN channels, under these conditions, will also display voltage hysteresis. We hypothesize that voltage hysteresis in HCN channels also stabilizes delta wave oscillations in

thalamic neurons. This type of voltage hysteresis in HCN channels may also play a role in generating and maintaining neuronal oscillations in spike wave epileptic seizures (Steriade et al., 1998; Timofeev et al., 2002).

APPENDIX 1

Description of the Four-state Model Used for SA-node Simulations

To explore the physiological role of the properties of HCN channels found in the present investigation, we used the following four-state model (which shows the size of voltage shifts more explicitly than the description used in Fig. 5 and in MATERIALS AND METHODS):

$$\begin{array}{ccc} & \beta_{II} & \\ O_{II} & \rightleftarrows & C_{II} \\ & \alpha_{II} & \\ \kappa_O \uparrow\downarrow \lambda_O & & \kappa_C \uparrow\downarrow \lambda_C \\ & \beta_I & \\ O_I & \rightleftarrows & C_I, \\ & \alpha_I & \end{array}$$

where O and C denote open and closed states, respectively, I and II denote modes I and II, respectively. α_i and β_i are described by

$$\alpha_i = k_{1/2}\exp(-ze_0(V-V_i)/kT) \quad \text{(A1)}$$

$$\beta_i = k_{1/2}\exp(+ze_0(V-V_i)/kT), \quad \text{(A2)}$$

where $k_{1/2}$ is the rate constant at $V = V_i$ (when $\alpha = \beta$), z is the valency of the transition, e_0 is the elementary charge, V is the membrane voltage, k is Boltzmann's constant, and T is the absolute temperature; i indicates mode I or II. The absolute values of V_i were chosen to obtain a 50% open probability at −75 mV (=[$V_I + V_{II}$]/2), similar to other published HCN channel models (Zhang et al., 2000; Altomare et al., 2001). Thus, $V_I = -75 - \Delta V_{mode}/2$, and $V_{II} = -75 + \Delta V_{mode}/2$. For example, we used $V_I = -105$ and $V_{II} = -45$, to achieve a 60-mV mode shift ($\Delta V_{mode} = V_{II} - V_I$). We used z = 1, which was also found for most HCN channel models. $k_{1/2}$ was set to 20 s^{-1} to generate reasonably fast opening kinetics. $\kappa_O = \lambda_C = 10\ s^{-1}$ because the time constant for the mode shift was ~100 ms at saturating voltages:

$$\kappa_O = \lambda_C = 10\ s^{-1} \quad \text{(A3)}$$

$$\lambda_O = \kappa_C = \kappa_O(\alpha_I\beta_{II}/(\alpha_{II}\beta_I))^{0.5} = \kappa_O\exp(-ze_0\Delta V_{mode}/kT). \quad \text{(A4)}$$

For a mode shift of 60 mV, λ_O and κ_C are 0.92 s^{-1}.

APPENDIX 2

Extension of the Four-state Model to a 20-state Model

We have mainly used a simple four-state model, since it can qualitatively describe most of the experimental data presented in this paper. A natural expansion of the four-state model would include four additional closed states and four additional open states for each mode, by allowing S4 in each subunit to move independently in each state. The resulting 20-state model (Fig. 20 A) would be able to generate the voltage hysteresis described in this paper, in addition to the sigmoidicity of the activation and deactivation currents. Determining a unique set of parameters for the 20-state model would require significantly more kinetic data. We have, therefore, left the development of this model for a future study. However, we point out now that, with this simple extension of the four-state model to the 20-state model, voltage hysteresis can generate the qualitatively different tail currents shown in HCN channels (Fig. 20).

Slowing Versus Sigmoidicity during Tail Currents

The changes in the tail currents induced by longer prepulses were qualitatively different at different tail potentials. At tail potentials close to $V_{1/2}$, the changes were mainly expressed as a slowing of the time constant, while at more depolarized tail potential, the changes were mainly expressed as an increase in sigmoidicity. The four-state model can replicate the slowing of the tails, but not the change in sigmoidicity. The sigmoidicity suggests that in any complete HCN channel model, there has to be at least four open states. The 20-state model, which has five open states in each mode, can reproduce the different changes in the tail currents at different potentials (Fig. 20, B and C). We assume that voltage hysteresis mainly affects the transitions between closed (α) or open states (β) and that the voltage dependence of the open-to-close transition is less than the voltage dependence of the transitions between open states, thus rendering the open-to-close transition rate limiting at depolarized potentials.

At depolarized potentials, the transitions between open states in mode I are faster than the last open-to-close transition, leading to a tail kinetics that is, roughly, a single exponential. After the channels have shifted into mode II, the transitions between open states are slower (now similar in kinetics to the open-to-close transition), which introduces a sigmoidicity in the tail kinetics without significantly slowing the time constant of the tail currents at depolarized potentials. At less depolarized tail potentials, the transitions between open states in mode I are similar to the last open-to-close transition, leading to tail kinetics that have some

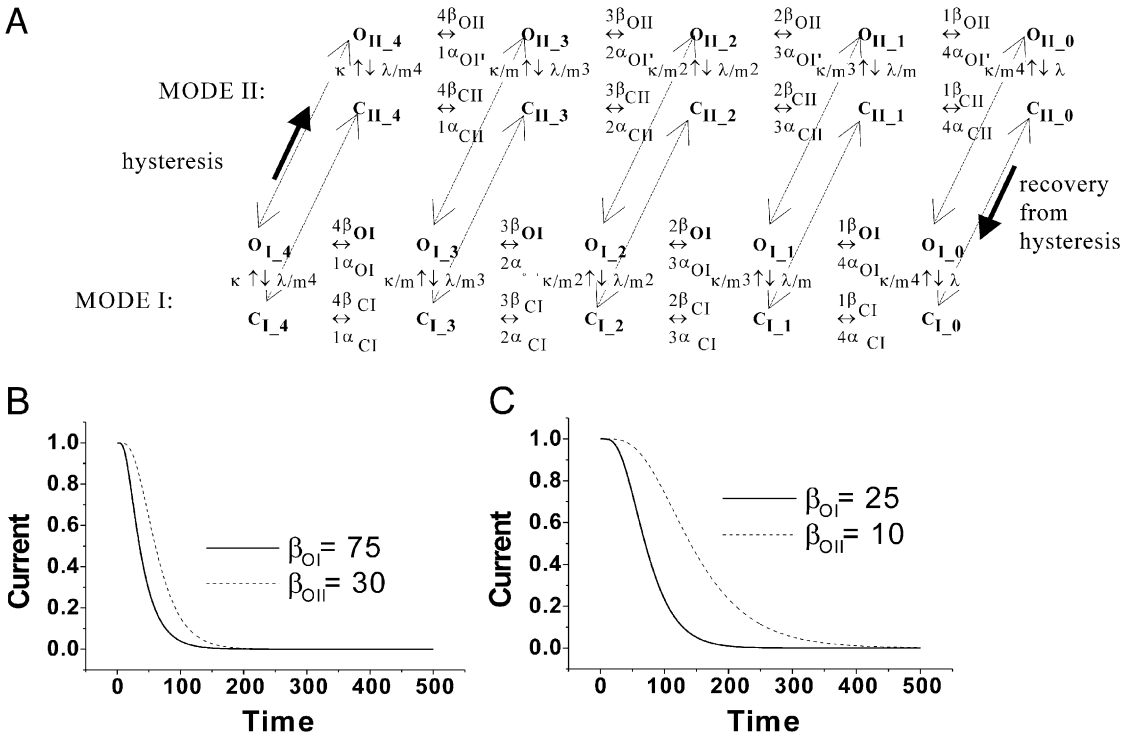

FIGURE 20. 20-state extension of the four-state model. (A) Each closed and open state in the four-state model have been expanded to five states, representing 0, 1, 2, 3, or 4 S4s activated (moved inward). The channels would mainly open from the states with all S4s activated and close from the states with all S4s deactivated (moved outward). Hysteresis mainly affects the α and β rates. (B and C) Simulations of tail currents after short (continuous line) and long (dotted line) activation prepulses, using a simplified version of the model in A. All channels were assumed to be in O_i4 after short prepulses and in $O_{ii}4$ after long prepulses. For simplicity, all rate constants were assumed to be zero except for β and λ. The closing rate λ is set to 25 ms^{-1} for all traces. β was assumed to change 2.5-fold between mode I and mode II. (B) Tail currents at +50 mV, where β = 75 ms^{-1} in mode I. (C) Tail currents at −15 mV, where β = 25 ms^{-1} in mode I. These simple simulations are not supposed to be seen as a quantitative fit to our recordings, but only as a qualitative suggestion that the slowing of the tails and the development of a delay in the tails can be due to voltage hysteresis. For example, the voltage dependence in these simulations was assumed to be only in the closed–closed transitions and open–open transitions, not in the open–closed transitions. Most likely, the open–closed transitions are also voltage dependent (Altomare et al., 2001).

sigmoidicity already in mode I. At less depolarized potentials in mode II, the transitions between open states are slower than the open-to-close transition, which will mainly lead to a slowing of the tail kinetics.

We thank Dr. U.B. Kaupp (Forschungszentrum Julich, Julich, Germany) for providing the spHCN clone; Drs. P. Århem, L. Brown, J. Karpen, J. Maylie, S. Johansson, and B. Rydqvist for comments on the manuscript; Dr. Sandra Oster for editing the manuscript; and Drs. L. Bergfeldt, G. Kennebäck, B. Eriksson, and colleagues in the Cardiology Sections at Karolinska Hospital and Huddinge Hospital in Stockholm for discussions.

This study was supported by grants from the Swedish Research Council (no. 13043 to F. Elinder), Åke Wibergs Stiftelse (F. Elinder), Magn. Bergvalls Stiftelse (F. Elinder), The Swedish Society of Medicine (F. Elinder), and National Institutes of Health (grant NS043259 to H.P. Larsson). R. Männikkö was supported by a predoctoral grant from the National Network in Neuroscience in Sweden.

Olaf S. Andersen served as editor.

Submitted: 18 June 2004
Accepted: 14 January 2005

REFERENCES

Aggarwal, S.K., and R. MacKinnon. 1996. Contribution of the S4 segment to gating charge in the Shaker K^+ channel. *Neuron.* 16: 1169–1177.

Altomare, C., A. Bucchi, E. Camatini, M. Baruscotti, C. Viscomi, A. Moroni, and D. DiFrancesco. 2001. Integrated allosteric model of voltage gating of HCN channels. *J. Gen. Physiol.* 117:519–532.

Armstrong, C.M., and F. Bezanilla. 1973. Currents related to movement of the gating particles of the sodium channels. *Nature.* 242: 459–461.

Baruscotti, M., and D. DiFrancesco. 2004. Pacemaker channels. *Ann. NY Acad. Sci.* 1015:111–121.

Bezanilla, F., E. Perozo, D.M. Papazian, and E. Stefani. 1991. Molecular basis of gating charge immobilization in Shaker potassium channels. *Science.* 254:679–683.

Bezanilla, F., R.E. Taylor, and J.M. Fernandez. 1982. Distribution and kinetics of membrane dielectric polarization. 1. Long-term inactivation of gating currents. *J. Gen. Physiol.* 79:21–40.

Clapham, D.E. 1998. Not so funny anymore: pacing channels are cloned. *Neuron.* 21:5–7.

Cole, K.S., and J.W. Moore. 1960. Ionic current measurements in the squid giant axon membrane. *J. Gen. Physiol.* 44:123–167.

DiFrancesco, D. 1984. Characterization of the pace-maker current kinetics in calf Purkinje fibres. *J. Physiol.* 348:341–367.

DiFrancesco, D. 1993. Pacemaker mechanisms in cardiac tissue. *Annu. Rev. Physiol.* 55:455–472.

DiFrancesco, D., and A. Ferroni. 1983. Delayed activation of the cardiac pacemaker current and its dependence on conditioning pre-hyperpolarizations. *Pflugers Arch.* 396:265–267.

Gauss, R., R. Seifert, and U.B. Kaupp. 1998. Molecular identification of a hyperpolarization-activated channel in sea urchin sperm. *Nature.* 393:583–587.

Hahin, R. 1988. Removal of inactivation causes time-invariant sodium current decays. *J. Gen. Physiol.* 92:331–350.

Hille, B. 2001. Ion Channels of Excitable Membranes. 3rd ed. Sinauer Associates, Inc., Sunderland, MA. 814 pp.

Hodgkin, A.L., and A.F. Huxley. 1952. A quantitative description of membrane current and its application to conduction and excitation in nerve. *J. Physiol.* 117:500–544.

Keynes, R.D., and F. Elinder. 1999. The screw-helical voltage gating of ion channels. *Proc. R. Soc. Lond. B. Biol. Sci.* 266:843–852.

Keynes, R.D., and E. Rojas. 1974. Kinetics and steady-state properties of the charged system controlling sodium conductance in the squid gint axon. *J. Physiol.* 239:393–434.

Larsson, H.P. 2002. The search is on for the voltage sensor-to-gate coupling. *J. Gen. Physiol.* 120:475–481.

Larsson, H.P., O.S. Baker, D.S. Dhillon, and E.Y. Isacoff. 1996. Transmembrane movement of the Shaker K^+ channel S4. *Neuron.* 16:387–397.

Larsson, H.P., and F. Elinder. 2000. A conserved glutamate is important for slow inactivation in K^+ channels. *Neuron.* 27:573–583.

Liu, Y., M.E. Jurman, and G. Yellen. 1996. Dynamic rearrangement of the outer mouth of a K^+ channel during gating. *Neuron.* 16: 859–867.

Loots, E., and E.Y. Isacoff. 1998. Protein rearrangements underlying slow inactivation of the Shaker K^+ channel. *J. Gen. Physiol.* 112:377–389.

López-Barneo, J., T. Hoshi, S.H. Heinemann, and R.W. Aldrich. 1993. Effects of external cations and mutations in the pore region on C-type inactivation of Shaker potassium channels. *Receptors Channels.* 1:61–71.

Ludwig, A., X. Zong, M. Jeglitsch, F. Hoffmann, and M. Biel. 1998. A family of hyperpolarization-activated mammalian cation channels. *Nature.* 393:587–591.

Luthi, A., and D.A. McCormick. 1998. H-current: properties of a neuronal and network pacemaker. *Neuron.* 21:9–12.

Männikkö, R., F. Elinder, and H.P. Larsson. 2002. Voltage-sensing mechanism is conserved among ion channels gated by opposite voltages. *Nature.* 419:837–841.

Ogielska, E.M., W.N. Zagotta, T. Hoshi, S.H. Heinemann, J. Haab, and R.W. Aldrich. 1995. Cooperative subunit interactions in C-type inactivation of K channels. *Biophys. J.* 69:2449–2457.

Olcese, R., R. Latorre, L. Toro, F. Bezanilla, and E. Stefani. 1997. Correlation between charge movement and ionic current during slow inactivation in Shaker K^+ channels. *J. Gen. Physiol.* 110:579–589.

Olcese, R., D. Sigg, R. Latorre, F. Bezanilla, and E. Stefani. 2001. A conducting state with properties of a slow inactivated state in a *Shaker* K^+ channel mutant. *J. Gen. Physiol.* 117:149–163.

Panyi, G., Z.F. Sheng, L.W. Tu, and C. Deutsch. 1995. C-type inactivation of a voltage-gated K^+ channel occurs by a cooperative mechanism. *Biophys. J.* 69:896–903.

Pape, H.C. 1996. Queer current and pacemaker: the hyperpolarization-activated cation current in neurons. *Annu. Rev. Physiol.* 58: 299–327.

Santoro, B., and G.R. Tibbs. 1999. The HCN gene family: molecular basis of the hyperpolarization-activated pacemaker channels. *Ann. NY Acad. Sci.* 868:741–764.

Santoro, B., S. Chen, A. Luthi, P. Pavlidis, G.P. Shumyatsky, G.R. Tibbs, and S.A. Siegelbaum. 2000. Molecular and functional heterogeneity of hyperpolarization-activated pacemaker channels in the mouse CNS. *J. Neurosci.* 20:5264–5275.

Seoh, S.-A., D. Sigg, D.M. Papazian, and F. Bezanilla. 1996. Voltage-sensing residues in the S2 and S4 segments of the Shaker K^+ channel. *Neuron.* 16:1159–1167.

Shin, K.S., C. Maertens, C. Proenza, B.S. Rothberg, and G. Yellen. 2004. Inactivation in HCN channels results from reclosure of the activation gate: desensitization to voltage. *Neuron.* 41:737–744.

Steriade, M., F. Amzica, D. Neckelmann, and I. Timofeev. 1998. Spike-wave complexes and fast components of cortically generated seizures. II. Extra- and intracellular patterns. *J. Neurophysiol.* 80:1456–1479.

Tchou, P.J., and M.K. Chung. 2000. Sick sinus syndrome and hypersensitive carotid sinus syndrome. *In* Cardiac Electrophysiology – From Cell to Bedside. D.P. Zipes and J. Jalife, editors. WB Saunders Company, Philadelphia. 862–873.

Timofeev, I., M. Bazhenov, T. Sejnowski, and M. Steriade. 2002. Cortical hyperpolarization-activated depolarizing current takes part in the generation of focal paroxysmal activities. *Proc. Natl. Acad. Sci. USA.* 99:9533–9537.

Vemana, S., S. Pandey, and H.P. Larsson. 2004. S4 movement in a mammalian HCN channel. *J. Gen. Physiol.* 123:21–32.

Wainger, B.J., M. DeGennaro, B. Santoro, S.A. Siegelbaum, and G.R. Tibbs. 2001. Molecular mechanism of cAMP modulation of HCN pacemaker channels. *Nature.* 411:805–810.

Wang, J., S. Chen, M.F. Nolan, and S.A. Siegelbaum. 2002. Activity-dependent regulation of HCN pacemaker channels by cyclic AMP: signaling through dynamic allosteric coupling. *Neuron.* 36: 451–461.

Yang, N., A.L. George, and R. Horn. 1996. Molecular basis of charge movement in voltage-gated sodium channels. *Neuron.* 16: 113–122.

Yu, F.H., and W.A. Catterall. 2004. The VGL-Chanome: a protein superfamily specialized for electrical signalling and ionic homeostasis. *Sci. STKE.* 253:re15.

Zagotta, W.N., T. Hoshi, and R.W. Aldrich. 1994. Shaker potassium channel gating III: evaluation of kinetic models for activation. *J. Gen. Physiol.* 103:321–362.

Zhang, H., A.V. Holden, I. Kodama, H. Honjo, M. Lei, T. Varghese, and M.R. Boyett. 2000. Mathematical models of action potentials in the periphery and center of the rabbit sinoatrial node. *Am. J. Physiol. Heart Circ. Physiol.* 279:H397–H421.